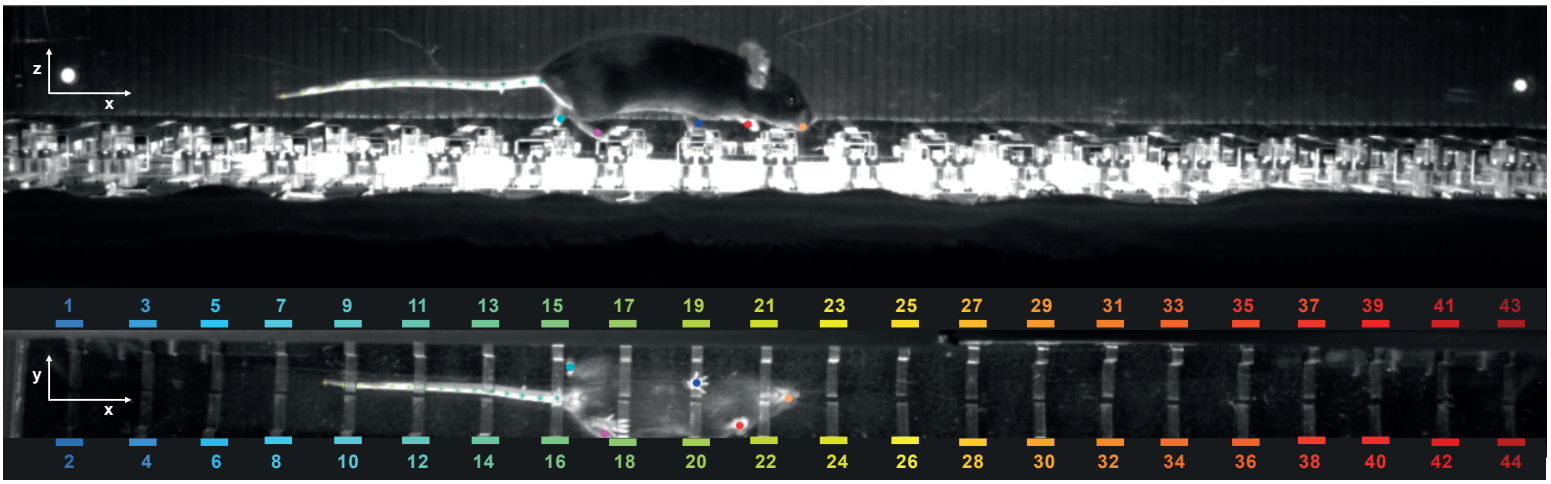

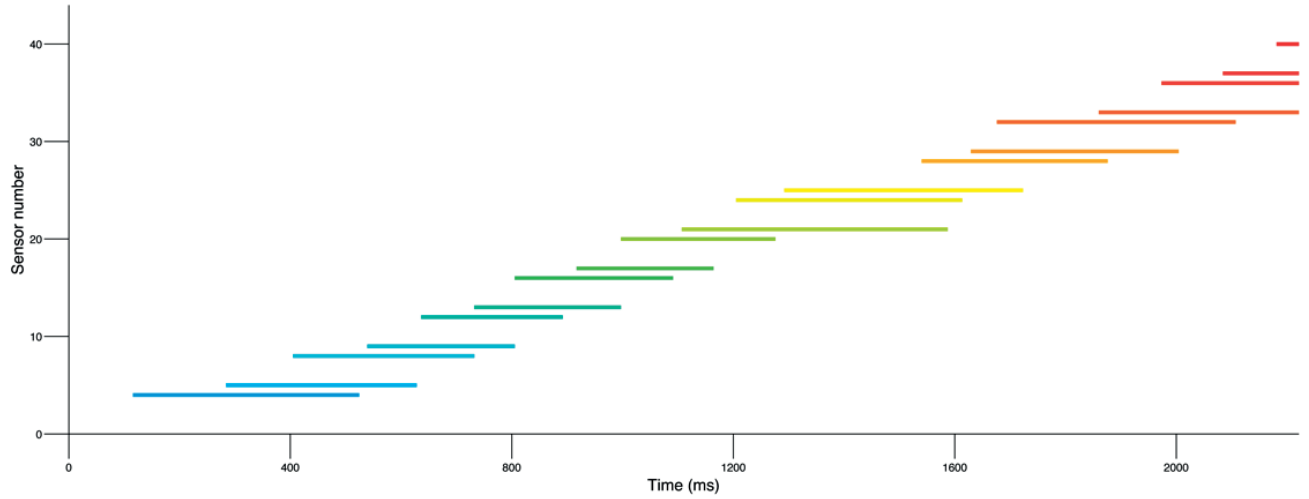

Gonçalo Gil Chaves Figueira

A LADDER PARADIGM FOR STUDYING LOCOMOTOR COORDINATION IN MICE

A dissertation submitted in fulfillment of the requirements for the degree of Master of Science in Biomedical Engineering at the University of Coimbra

February 2016

· U C ·

Universidade de Coimbra

• U C •

FCTUC FACULDADE DE CIÊNCIAS
E TECNOLOGIA
UNIVERSIDADE DE COIMBRA

Gonçalo Gil Chaves Figueira

A ladder paradigm for studying locomotor coordination in mice

A dissertation submitted in fulfillment of the requirements
for the degree of Master of Science in Biomedical Engineering
at the
University of Coimbra

Supervisor:
Megan Carey, Ph.D

Co-supervisor:
Miguel Castelo-Branco, M.D, Ph.D

Coimbra, 2016

This work was developed in collaboration with:

Champalimaud Foundation

Champalimaud Foundation – Lisbon, Portugal

Institute for Biomedical Imaging and Life Sciences – Coimbra, Portugal

Para ti Pai, Para ti Mãe

Any sufficiently advanced technology is indistinguishable from magic.
Arthur C. Clarke, "Profiles of The Future", 1961 (Clarke's third law)

Acknowledgements

First, I would like to give a big thank you to Dr. Megan Carey for the opportunity to develop such project and especially for all the guidance, teaching and constant support throughout this year. A thank you to Dr. Miguel Castelo-Branco, for the motivation to do this work. I also would like to thank Dr. Miguel Morgado for all the help provided. I extend to them my grateful sincere admiration.

I indeed want to express my gratitude to the people in the lab, from whom I learned so much. They are indeed responsible for the creation of such an incredible environment. Ana; Dana; Catarina; Tatiana; Tracy; Dominique; Hugo; Jovin; Dennis; João Freitas and João Cruz. Without their collaboration, nothing of this would have been possible.

A special thank you to my non-madeiran and madeiran friends that are still with me after these five years enriched by extraordinary experiences. The ones that got here are the ones that prosper throughout life.

Last but not the least, to my family. A warm thank you to my parents for always believing in me. This project is dedicated to them for a reason. As a wise man once said, “do not ever forget your origins”.

Abstract

The apparent fluent capacity to generate competent movement is a remarkable feature of the intricate information processing that takes place in the brain. Since movement is the ultimate result of processes carried out by the motor system, behavioral experiments are crucial to understand how the brain generates complex body movements. The cerebellum is essential for an accurate and coordinated gait. However, it is still a poorly understood component of the motor system.

Our laboratory has previously established a quantitative framework for studying mouse locomotor coordination during overground walking (Machado and Darmohray et al., 2015).

In the present project, we have developed the *LocoLadder,* which comprises a horizontal ladder coupled with force sensors, designed to measure the load exerted by the paws of mice as they traverse the ladder. This was complemented by tracking of mice body parts with high spatiotemporal resolution for measuring locomotor patterns of interest. Using this system, we were able to successfully characterize the locomotor profiles of both wildtype and cerebellar ataxic reeler mice, allowing us to highlight the locomotor deficiencies in the latter.

Taken together, the association of load and gait assessment represents a significant step toward sensitively quantify locomotor coordination in a ladder configuration. Such a system combined with new optogenetic tools should yield relevant details about motor control and provide new means of understanding how the cerebellum contributes to skilled locomotion.

Keywords: Motor coordination; Locomotion; Ladder; Force sensors.

Resumo

A aparente simplicidade de gerar movimento capaz, é uma característica notável do processamento complexo de informação que tem lugar no nosso cérebro. Pelo facto de o movimento ser o resultado final dos processos desempenhados pelo sistema motor, as experiências comportamentais são cruciais para explicar como é que o cérebro gera movimentos corporais complexos. Sabe-se que o cerebelo é fundamental para uma marcha coordenada e exacta. Contudo, é ainda uma estrutura pouco conhecida do sistema motor.

No laboratório foi previamente desenvolvida uma nova abordagem quantitativa para o estudo da coordenação motora em ratinhos durante a marcha em superfície plana e contínua (Machado and Darmohray et al. 2015).

No presente projecto, foi desenvolvido um sistema, denominado *LocoLadder*, que inclui uma escada horizontal acoplada a sensores de pressão, com o propósito de aceder à força exercida pelas patas nos degraus, ao longo do percurso do ratinho pela escada. Este sistema foi complementado com o registo do percurso das diferentes partes do corpo do ratinho com elevada resolução espácio-temporal, para medição de padrões locomotores de interesse. Utilizando este método experimental, caracterizou-se também, com sucesso, o perfil locomotor dos ratinhos controlo e dos ratinhos *reeler* com ataxia cerebelar, tendo sido possível identificar várias incapacidades locomotoras nos últimos.

Em suma, a associação da medição da pressão exercida pelas patas com a análise da marcha, permitiu uma melhor quantificação sensitiva da coordenação locomotora em escada. Pensamos que, este sistema combinado com os novos métodos de optogenética, poderão fornecer detalhes relevantes sobre o controlo motor e proporcionar novas formas para compreender como é que o cerebelo contribui para a locomoção hábil.

Palavras-chave: Coordenação motora; Locomoção; Escada; Sensores de pressão.

List of Figures

List of Tables

Index

Chapter 1

Introduction

The present chapter includes a description of the underlying principles of motor function with particular focus on the role of the cerebellum in motor control. Next, the state of the art of motor behavioral tasks for rodents and respective strengths and limitations for studying locomotion are discussed. Finally, the main objectives and the thesis organization are highlighted. This work was developed at the Neural Circuits and Behavioral Laboratory in Champalimaud Foundation during the final year of the Biomedical Engineering Integrated Masters.

1.1 Locomotion: an elegant intricacy

How does the brain generate movement? Scientists from many different fields have been trying to solve this query. However, we are still far from having a clear picture. The simplicity with which we perform everyday motor tasks hides the real elaboration of the control mechanisms at stake. For instance, human-like movements are hardly executed by our programmed machines. Although they have proved a striking capacity to defeat world-champions at chess, [1] no robot

can yet handle a chess piece with the proficiency of a child [2].

Deciding when and how to perform a movement is, to a great extent, what triggered the progression of the nervous system. The power to move from on place to another is a crucial feature of animal survival. Locomotion is therefore involved in a variety of essential behaviors, such as the hunting for food, the competence to localize mates or to run from predators, or the response to stress [3].

The apparent fluent capacity to generate competent movement is a remarkable feature of the intricate information processing that takes place in the brain. Movement is a result of the interplay within the sensory systems, information processing, coordinated muscle activity that follows appropriate motor commands, and ultimately the interaction between body parts and the surroundings [3]. How is neural activity orchestrated within different brain structures to control different aspects of movement?

The elements within the motor system need to have access to the continuously flow of sensory information. For instance, during stepping, several sensory modalities, comprising somatosensory input provided by the muscle and skin receptors, input from the vestibular system (for controlling balance), and a continuous stream of visual information, are essential to generate an appropriate motor output [3]. But where in the brain are these sensorimotor transformations generated? What sequence of events occur between the integration of sensory cues and the motor output?

Mammalian locomotion frequently comprises rhythmic movements of the whole-body elements, however they are not necessarily rigid maneuvers [3]. Locomotor patterns are highly sensitive to environmental conditions and must be continually modified, usually in a subtle fashion, to accommodate variations in the immediate surroundings. In order to deal with such an unpredictable environment, limb movements have to be extraordinary flexible. Moreover, an

uninterrupted control of coordination within (intralimb), between (interlimb) the limbs and across the whole-body is crucial for a successful locomotion [4]. How do neural circuits change to adjust the locomotor movements relative to particular events in the environment?

Considering that movement is the visible output of the neural system, behavioral experiments are vital in order to explain how the brain works. Currently, we have at our disposal cutting-edge techniques to monitor and manipulate neural circuits that hold great potential to reveal what happens in the brain during behavior. Nevertheless, to tackle these questions, more controlled and sensitive behavioral tasks need to be developed [5,6].

1.2 Movement is orchestrated by multiple subsystems

The interactive process within various regions of the neural system is what makes our ordinary movements seem effortless. A system capable of generating movement relies on the existence of elements that receive input, process information and send the generated motor command to the effectors that produce the motor response. In the nervous system, the receivers are the sensory systems that transform physical input into an electrical signal through dedicated sensors on the periphery of the body. This signal is then sent to be processed by the brain through the afferent neurons. The motor command then travels through the motor efferent neurons towards the skeletal muscles (the effectors) that will produce the motor output. The motor areas involved in the process are organized in a functional hierarchy and participate in distinct levels of motor control [3].

The lowest degree of this functional organization is mediated by the spinal cord and brain stem, which are mostly concerned with the accurate execution of muscle actions. Inside the gray matter of the spinal cord lies the cell bodies of neurons called motor neurons and interneurons (Figure 1.1). A single motor neuron might directly receive an enormous amount of inputs from motor brain regions through the white matter of the spine. Alternatively, interneurons can intermediate these connections, allowing intricate circuits to emerge. The motor neurons project to the muscles, being responsible for the final common path of movement. While analyzing the remaining functionalities of the spinal cord after being disconnected from the brain, it was found that it comprises the elements for producing involuntary, simple and coordinated movements. These local spinal circuits, called central pattern generators, are sufficient to generate the basic motor pattern for locomotion. However, when more precise movements are required, such as stepping on a grid, additional information from other motor control pathways is needed for effective locomotion [3,7,8].

Prior to the actual execution, the motor command has to be carefully shaped by upper structures in the brain that are concerned with particular aspects of movement. One of the principal brain regions involved in motor control is the motor cortex by modulating an array of descending pathways. The motor cortex is subdivided into a group of structures that are concerned with high-level movement features. By being closely interconnected with brain regions that integrate sensory information, it transforms the plan of action into the motor commands that execute the program. The motor cortex is also involved in coordinating the sequence of movements, context-dependent motor action selection and in the execution of complex sequence of movements [3].

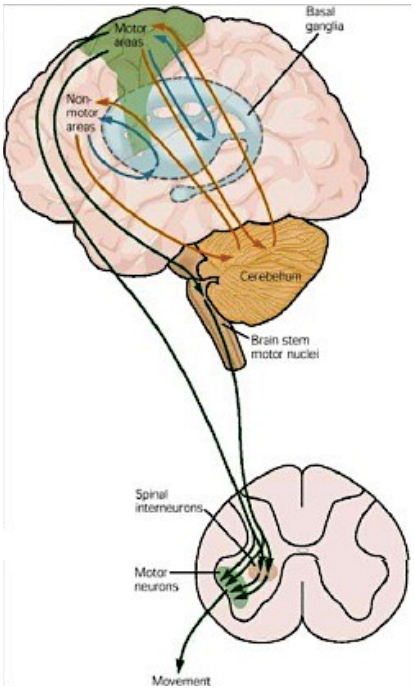

Figure 1.1: Organization of the motor system. Highly interactive motor structures participate in distinct levels of motor control. Adapted from [3].

There are also two important structures that shape the motor output by establishing side loops connections with other structures of the motor system. One of them is the basal ganglia (Figure 1.1). It comprises a group of subcortical structures that appear to be involved in the enabling of motor actions. Through projections via the thalamus to the motor cortex, the basal ganglia seems to be involved in triggering the initiation of voluntary movements [3].

The other structure is cerebellum, which is thought to be important in correcting subtle aspects of the ongoing movement. The cerebellum influences, via brain stem, the low-level motor control provided by the spinal cord and also establishes several connections with the motor cortex via the thalamus. This structure plays a role in the planning and timing of movements [3].

Moreover, the cerebellum seems to integrate sensory information with motor commands to generate adaptive motor coordination. This integrated input might be used to construct predictive models to anticipate the consequences of a motor action. For instance, due to the several segments of an arm, the movement

of the forearm alone forces the upper arm to move as well. In order for a healthy person extend the elbow while keeping their shoulder still, the muscles controlling shoulder displacements must contract to inhibit its passive movement. Patients with lesions in the cerebellum cannot counterbalance these interaction forces. The cerebellum might use these internal models to anticipate and counterbalance the forces caused by the physical structure of the limb, resulting in a smooth and efficient movement. However, it is still unknown how internal models are embedded within cerebellar circuitry [3].

1.3 Cerebellar organization and circuitry

The cerebellum is located at the base of the skull, dorsally to the brainstem. The two main anatomical structures of the cerebellum are the cortex and the deep cerebellar nuclei, which are constituted by gray and white matter, respectively. The superficial part of cerebellar cortex has an enormous area due to the presence of many parallel folds called folia [9]. The deep cerebellar nuclei comprises three pairs of nuclei: the fastigial nucleus, the interposed nucleus (which includes the emboliform and globose nucleus) and the dentate nucleus (Figure 1.2 A) [3].

The cerebellum is connected to the brainstem through three symmetrical pair of tracts: inferior, middle and superior cerebellar peduncles (Figure 1.2 B). Because the inputs are ipsilateral regarding their entrance side into the brainstem, the cerebellum is unique compared to most structures of the brain: the right cerebellum is concerned with the right half of the body and the left cerebellum the left half [5].

Currently, it is thought that cerebellar regions have distinct roles in controlling locomotion and balance. Functionally, the cerebellum is divided into three different areas: the spinocerebellum, cerebrocerebellum and vestibulocerebellum (Figure 1.2 C). The spinocerebellum is constituted by the medial (vermis) and intermediate zones of the hemispheres and receives ample tactile information from the spinal cord. It seems to be involved in posture and gait control, as well as eye movements. The cerebrocerebellum is composed by the lateral parts of the hemispheres and it is thought to participate in programming, coordination and learning of demanding motor tasks. Finally, the vestibulocerebellum appears to be mainly concerned with controlling balance and eye movements [3].

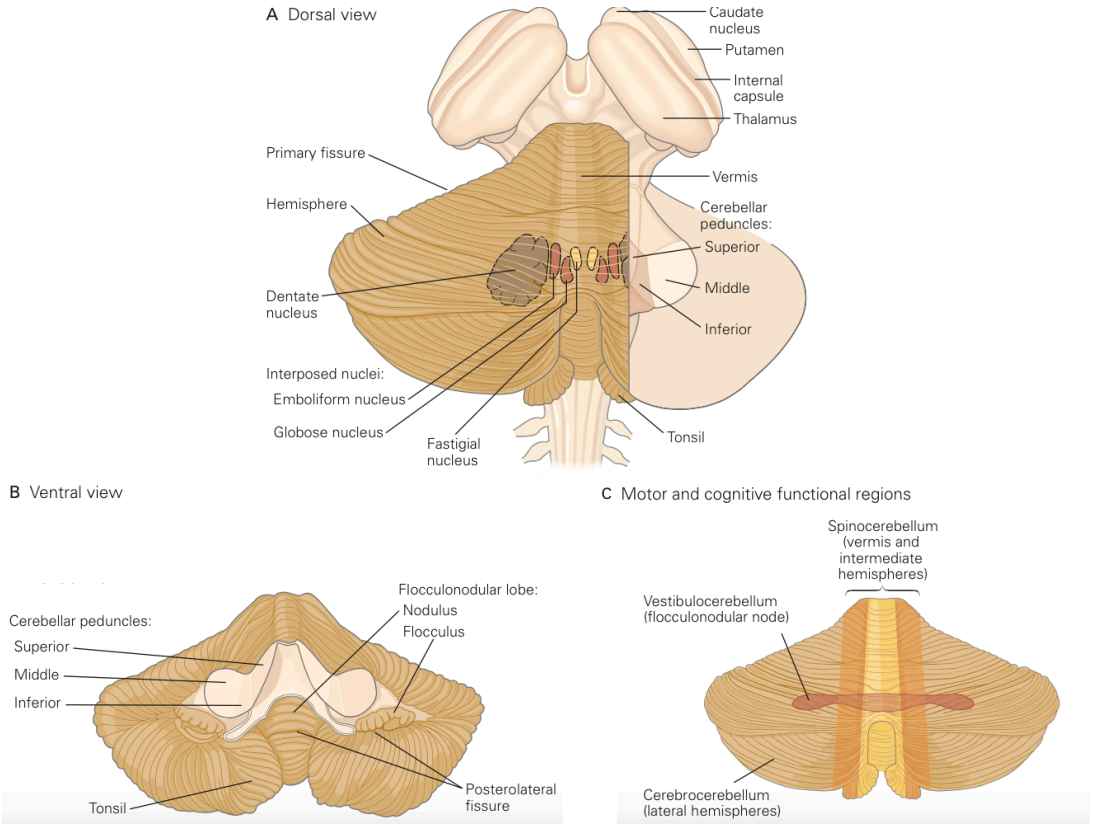

Figure 1.2: Overall organization of the human cerebellum. **A)** Dorsal view of the left hemisphere. The three pairs of deep nuclei are depicted in the picture. The deep nucleus is shown in the right hemisphere. **B)** Ventral view exhibiting the cerebellar peduncles. **C)** Functional cerebellar regions. Adapted from [3].

The cerebellar cortex is constituted by several types of neurons organized in three distinct layers: the molecular layer, Purkinje cell layer and the granular layer (Figure 1.3 A) [3].

The molecular layer of the cerebellar cortex contains mostly the parallel fibers that are formed by branching of the ascending axons of the granule cells, which are located in the granular layer. The parallel fibers cross the medial-lateral direction of the folia and make various connections with Purkinje cells. Also, the molecular layer comprises the cell bodies of two types of inhibitory interneurons, the stellate and basket cells, which receive excitatory input from the parallel fibers and inhibit Purkinje cells [3].

The Purkinje cells, whose cell bodies form the Purkinje cell layer located below the molecular layer, are the only output of the cerebellar cortex and provide inhibition to the deep cerebellar nuclei. Their dendrites expand upward into the molecular layer and are arranged perpendicular to the parallel fibers (in the anterior-posterior axis) (Figure 1.3 B) [3].

Within granular layer, granule cells receive inhibitory input from Golgi cells, which are also located in this layer. Importantly, granule cells also get excitatory input from mossy fibers, one of the two principal inputs of the cerebellum. These fibers have their cell bodies in the spinal cord and brain stem and transmit sensory signals from the periphery as well as information from the cerebral cortex. Thus, mossy fibers are thought to be fundamental for transmitting not only detailed information about movements, (for example direction, force and speed) and touch information, but also features regarding motor commands delivered by the cerebral cortex. This information is then distributed and encoded in different granule cells. A huge amount of granule cells synapse to a single Purkinje cell, modulating its activity via parallel fibers. Thus, the granular layer is responsible for integrating multiple inputs that will influence

the next processing level carried out by the Purkinje cells [3]. Thus, the function of downstream cerebellar circuit is then completely dependent on the computation performed by the granular layer, determining, to a great extent, the cerebellar function.

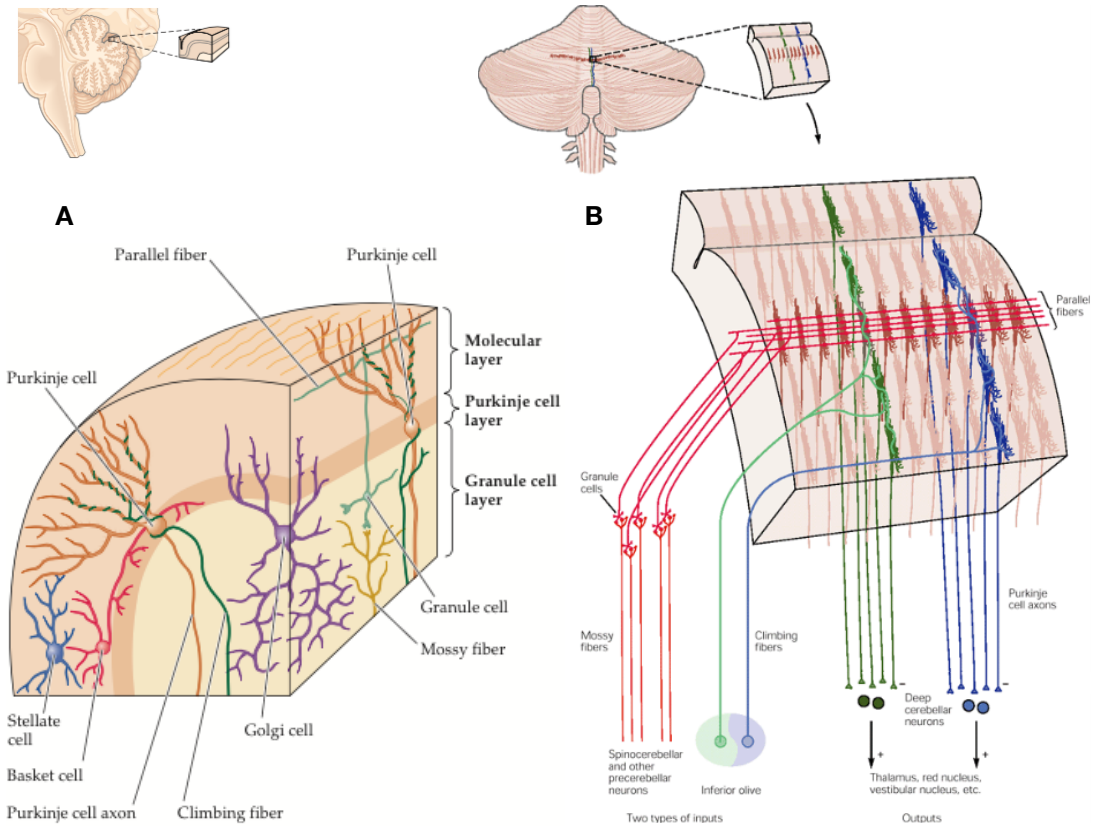

Figure 1.3: Cerebellar circuits. **A)** General organization of the cerebellar cortex. The different neurons are depicted in the different layers. **B)** Perpendicular arrangement of the mossy and parallel fiber system. The climbing fiber input is also shown. Purkinje cells deliver the only output of cerebellar cortex to the deep cerebellar nuclei. Adapted from [3,5].

The other major input to the cerebellum is the climbing-fiber input. It arises from the inferior olive and transmits sensory information from both the periphery and from the cerebral cortex. Each Purkinje cell connects to one single climbing fiber, contrasting with the abundant convergence of mossy fibers to granule cells [10]. Furthermore, contrary to the granule cells, climbing fibers cause a strong effect on Purkinje cell activity, which are normally related to specific

sensory occurrences. This fact suggests that these cells are specialized for event detection [3].

The output of cerebellar cortical processing is then transmitted to the deep cerebellar nuclei through Purkinje cells. Mossy fibers and climbing fibers also form excitatory connections with the cerebellar nuclei. This microcircuit represents the basic module present across the cerebellum (Figure 1.4) [3].

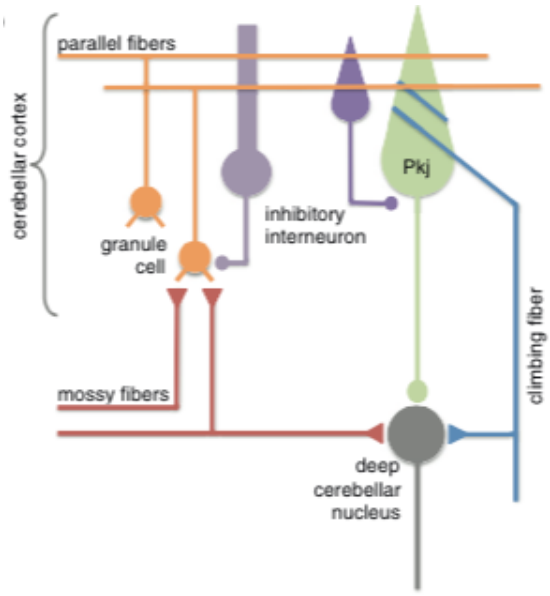

Figure 1.4: Illustration of the cerebellar circuit. The inputs and outputs, as well as the connections within cerebellar circuit elements are shown. The circular end shape code for inhibitory, whereas triangular shape for excitatory synapse. Adapted from [90].

1.4 Cerebellar dysfunction

Disorders of the cerebellum result in dysfunctional movement. Importantly, these patients exhibit movement disruption instead of losing the ability to move, which occurs in paralysis caused by cerebral cortex damage. Although we do not yet fully understand how cerebellar function maps to the symptoms visible in patients with cerebellar damage, these signs have been extensively identified and characterized [3].

In a healthy person, the leg usually comes to the initial point after a knee jerk induced by a tap on the patellar tendon. However, in cerebellar patients, the

leg might temporarily oscillate before returning to the initial state. This decreased resistance to neutral limb movement is called *hypotonia* [3].

These patients may also lose their ability to keep body posture or maintain a steady limb, which results in incapacity to walk or stand - *Astasia-abasia.* While moving, these patients tend to compensate by spreading their feet for stability [3].

Dysdiadochokinesia is clearly visible when a patient tries to execute rapid alternating motor actions. These patients fail to sustain a fixed rhythm or make a constant amount of force. Furthermore, when trying to reach a target, over and undershoot movements are typically observed– condition referred to as *dysmetria* [3].

In cerebellar *ataxia*, patients have difficulty producing smooth and properly coordinated movements. Furthermore, on the contrary, because motor sequences are poorly timed, movements are normally imprecise and unsteady. These abnormal movements are typically followed by excessive corrections – *hypermetria* – which enhances the overall disruption of ongoing motor coordination [11].

Because the cerebellum also shows involvement in the control of coordination and activation of agonist and antagonist muscles, the abnormal movements described often include a form of tremor at the end of the movement, (*intention tremor*) which normally occurs when the patient attempts to stop the ongoing motor action [3].

These phenotypes described are often seen after structural cerebellar damage in patients with a history of alcohol abuse and in paraneoplastic syndromes that follow certain types of cancer or genetic mutations [3,12-14]. Currently, besides regular rehabilitation to enhance motor abilities and providing means to live with the disease, there is no effective therapy [15].

1.5 Motor behavioral tasks for rodents

The cerebellum is clearly a fundamental, but still poorly understood, piece of the motor system. The activity within cerebellar circuit is modulated constantly during movement, generating patterns of neural activity in its neural elements that seem to correlate with different aspects of movement (for example, the direction of the movement) [5]. However, major questions remain: How is this information embedded within cerebellar circuitry elements?

Understanding how movements are controlled, such as walking, are an enormous challenge for recent research. Locomotion represents an excellent system to investigate how the cerebellum participates in motor control. All sort of mechanisms, from the generation of simpler walking patterns to more complex and fine control adjustments in coordination and balance are involved in locomotion. However, our knowledge is sparse regarding the contributions of specific cell types to more complex motor behaviors like locomotion [3].

Since movement is the ultimate result of processes carried out by the motor system, behavioral experiments are crucial to understanding how these motor brain structures contribute to the overall movement. Currently, there are several motor behavioral paradigms used to evaluate motor function. However, few behavioral systems are capable of properly characterizing specific aspects of locomotion. Thus, more controlled and highly sensitive behavioral tasks need to be created [5,6].

We not only need a better behavioral apparatus, but also to quantify locomotion in an experimental system capable of supporting neural circuit dissection. Human locomotion has been successfully investigated using motion capture and computational models [16,17]. Still, we do not have the appropriate tools to fully explore these questions in humans.

Currently, we have at our disposal advanced genetic tools to manipulate neural circuits in mice. These techniques have already been useful to explain how simple cerebellum-dependent behaviors work [18–20]. Indeed, they will certainly be crucial to unravel the mechanisms of complex behaviors, like locomotion. Moreover, the cerebellum role can be investigated by behaviorally testing mutant mice with specific abnormalities within the cerebellar circuit [15,21–23].

Mice are extremely active and exhibit a variety of movements that can be quantified using a relatively small apparatus. Moreover, some parallels can be made between aspects of human and rodent's locomotion; particularly in many basic features of motor control between bipedal and quadrupedal locomotion, [3] and in the fundamental mechanisms of skilled reaching movements [24]. Due to the increasing importance of using mouse models, the behavioral assays already developed for rats have been adapted for mouse usage [25].

The next sections will review the present behavioral paradigms available to evaluate motor function in rodents and discuss how they contribute to measure relevant aspects of locomotion. It is good to keep in mind that it is normally not enough to select a unique assay, because different tests assess different features of motor behavior. A specific behavioral test might be more relevant to quantify an aspect of movement. Also, more than one behavioral assay could be relevant to produce high quality data for the purpose of the experimental question. Motor behavioral assays can be categorized according to the main motor function that is assessed.

1.5.1 General battery tests

Several test batteries for fast examination of mice motor impairments have been created [26]. The SHIRPA (SmithKline Beecham, Harwell, Imperial College and Royal London Hospital phenotype assessment) is the most consistently

validated battery test. In this assay, mice are subjected to various simple tests that provide a standard screening for fast motor characterization [27].

Mice are normally placed in a transparent glass and their behavior is recorded using video capture. Typically, several observational measures are noted, including tremor, body location and natural activity [27].

Although this test is best suited to identify general motor problems in mice, it lacks sensitivity and does not provide sufficient distinction between individual motor parameters. These problems can be solved by using video analysis techniques. However, they limit the fast evaluation feature of these battery tests. Still, these assays are appropriate to a first evaluation of a group of mice with unidentified motor behavior.

1.5.2 Open-field

The most frequently used task to evaluate motor activity impairments is the open-field task [28]. The movements of the rodent are observed and recorded while it moves around an open space (Figure 1.5 A).

During the course of the test, the animal explores the square (or circular) arena while several measures are typically recorded by observation: The total distance traveled, [29] the number of edge and center regions entered, together with other natural behaviors [28]. Automatic video tracking or other detection technologies can be used to divide the explorative behaviors in specific aspects, enhancing the specificity of the open-field task [28].

Besides being a valuable tool to measure locomotor activity levels in mice, the open field activity test has been also useful to examine the effect of pharmacological substances on motor behavior and in studies of neuromuscular disease [29]. However, this test does not give quantified information about the causes of the motor dysfunction. Furthermore, several external factors, such as

cognition, anxiety and environmental conditions, might contribute to an increase in the variability in motor behavior, which masks the desired motor output [29]. Nonetheless, it can still be helpful as a complementary test to other more suitable motor paradigms.

1.5.3 Wheel running

Another method to evaluate locomotor activity is by measuring the propensity of mice to run in a running wheel installed in their home cage (Figure 1.5 B). In studies using running wheels, great amount of data can be automatically produced by measuring the total number of wheel revolutions, (distance travelled) the running velocity, (rotations per minute) the time to start running and the number of breaks from running [28]. Despite being a good tool to access generic physical activity, for example to access how active a mouse is, [30] it lacks sensitivity to measure particular details of locomotor behavior.

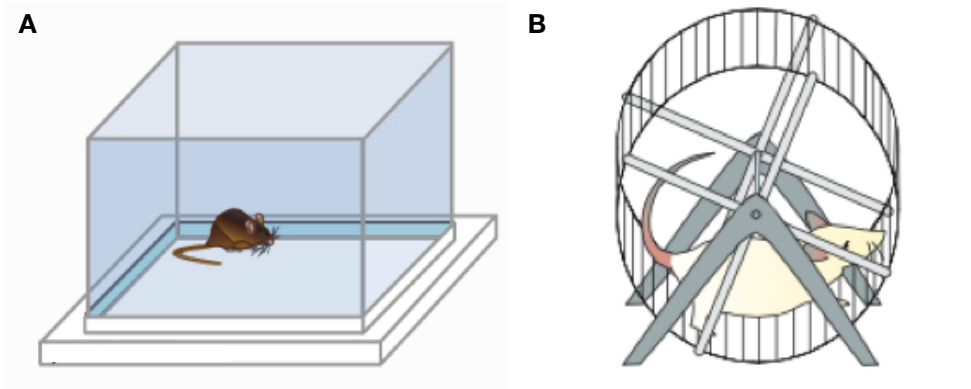

Figure 1.5: Locomotor activity tests. **A)** The mouse is placed inside an open-field while video tracking systems can be used to analyze locomotor activity parameters. **B)** Voluntary motor activity is assessed by placing a running wheel in a mouse's home cage. Adapted from [28,91].

1.5.4 Balance beam

In this task, while a mouse crosses a narrow beam, its capability to keep balance before reaching a shelter is assessed (Figure 1.6 A). The latency to transverse the beam and the number of paw slips are normally recorded. Some adaptations of this task included cross sections and diameters to change the difficulty of the test. Other versions used inclined beam or others that become increasingly narrower as it reaches the shelter [31].

Although this technique has been valuable in assessing motor coordination and balance in several mice studies, this paradigm gives only a general evaluation of possible balance and coordination deficits. Therefore, more sensitive test should be use to assess specific aspects of those motor problems [31]. Furthermore, motivational issues and excessive training can make mice uncooperative, introducing problems in the assessment of motor coordination.

1.5.5 Climbing

In the climbing task, a mouse is typically positioned on an inclined or upright pole, (Figure 1.6 B) which will trigger a specific escape reaction (such as climbing) in healthy animals. Several aspects of the behavioral response adopted, such as its latency, efficiency and carefulness with which it performs the task, are recorded for further analysis [28].

While a healthy mouse normally grasps the pole before turning around and gradually descends to the ground, a motor impaired mouse might climb or fall from the pole [28]. Although climbing is a rather simple test of motor dysfunction, it does not specify details regarding the actual motor deficiency. Moreover, because various features of motor function are used while climbing, the specificity to a particular aspect of motor behavior is reduced.

1.5.6 Rotarod

The rotarod is one popular behavioral tasks to evaluate motor function in mice in an automated way. The mouse is positioned on a rotating rod and has to keep its balance (Figure 1.6 C); a sensor embedded on the ground below registers the time duration until the mouse loses balance and falls from the rotating rod. In this test, several fixed velocities can be defined on separate trials, or an accelerating version can be used, where speed increases within a trial [28].

There are several problems associated with this test. Firstly, when mice lose balance, they may try to grasp the beam, instead of falling from the apparatus. Furthermore, during longer experiments mice might not cooperate, as they learn that falling is harmless. Thirdly, animals with most severe motor coordination problems will quickly fall off the rotarod. In contrast, for mice that can maintain balance, the test will turn into an endurance task instead of primarily accessing motor coordination [32]. Finally, it has been shown that heavier mice perform worse than lighter mice [28].

The sensitivity of this behavioral paradigm to identify small changes has been questioned, particularly when mild motor dysfunctions are being evaluated [33]. The rotarod is a valuable tool to access general balancing and motor coordination problems, however it does not provide enough sensitivity to identify subtle changes in locomotor behavior.

1.5.7 Swimming

Swimming behavior is another behavior suitable to investigate coordination between limbs. The mouse is filmed while it swims across a transparent tank (Figure 1.6 D). The motor performance is quantified by manually accessing several parameters in the recorded movie: number of strokes

of each individual paw, swimming velocity and time to reach the safe platform [28].

Swimming is a sensitive paradigm of motor coordination in mice, however several confounds are associated with it. First, when mice are forced to swim, they normally display a wide variety of motor behaviors due to their anxiety that does not reflect natural locomotion. Secondly, although there are some commercial automated behavior analysis systems available, these are far from being fully automated, requiring time-consuming inspection of the movies recorded [34]. Finally, if the motor deficits are too severe, there is a possibility of drowning, therefore extra vigilance is needed [28].

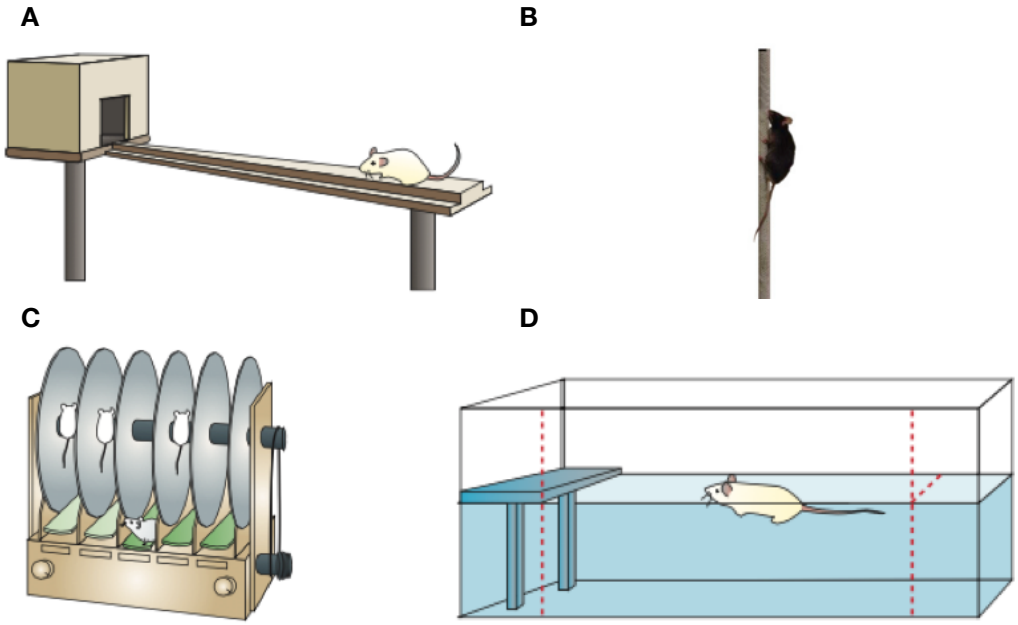

Figure 1.6: Balance and motor coordination tests. **A)** In the balance beam task, a mouse has to cross a narrow beam while their balance is assessed. **B)** A mouse is positioned on a pole while several aspects of its response are noted. **C)** Swimming test. The number strokes per paw and the latency finish are inspected in the movie recorded. **D)** The rotarod test. The primary parameter of motor coordination is the latency to fall from the apparatus. Adapted from [28,92].

1.5.8 Ground reaction forces

Ground reaction force assessment has been useful for analyzing motor behavior in a wide diversity of animals including rodents [35–41].

Due to the broad use of rodents in musculoskeletal diseases research, force sensor technologies have been currently used to study the locomotor behavior of these small animals. They are normally built in a plate-configuration (Figure 1.7). The animal is placed on the plate and its motor actions are detected by the force sensor elements located on the ground. The output signal of these load cells provides assessment of several motor features, such as locomotor activity [38,42,43], impact forces, (Figure 1.7 A) [36] and whole-body tremor (Figure 1.7 B) [38,44]. Furthermore, they have been implemented in other motor task, such as the overground walking, (Figure 1.7 C) [45,46] or running wheel [47].

While a mouse walks, each limb provides the support needed to maintain a correct whole-body posture at a regular speed [48]. The force sensors constitute a powerful tool to get insight into how these weight signatures contribute to the whole-body dynamics and locomotion by having direct access to the load exerted by the limbs.

These tools have independent capability and provide objective quantitative results [46]. However, it requires a very sensitive system to fully measure the rather large magnitude forces executed by these small animals [42].

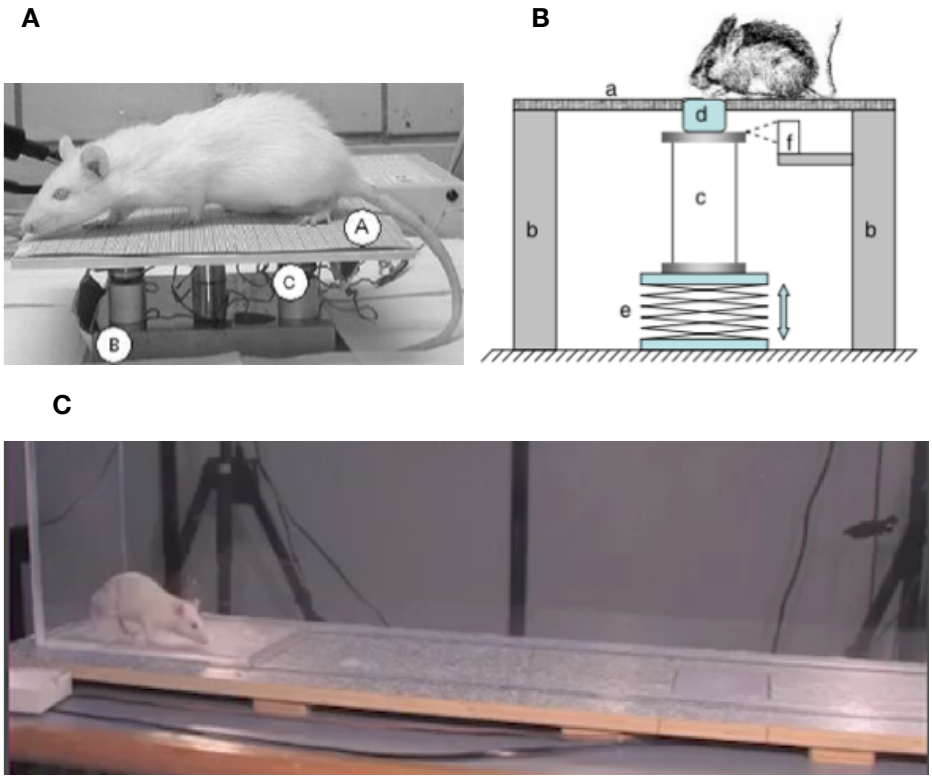

Figure 1.7: Examples of force sensors systems. **A)** Force sensor platform. Measures separate peak vertical impact forces produce by each paw when rat is dropped onto the platform. **B)** Force sensor for tremor analysis. The tremor is accessed through signal frequency analysis. **C**) Force sensors applied to overground walking task. The rodent crosses the corridor while force sensors embedded on the floor register vertical load. Adapted from [36,40,44].

1.5.9 Gait analysis

The gait inspection during natural walking enables almost a complete analysis of motor coordination. The most common task for evaluating mice gait is the footprint test (Figure 1.8 A). Each individual paw is painted with dyes of distinct colors. Then, mouse footprints are registered while it crosses over an appropriate footprint detection paper. Several gait parameters are extracted from the footprint patterns, such as stride length, overlap between fore and hind paws, width of base of support, and paw and digits splay [28].

Most of the tests described previously required continuous investigator attention and suffer from limitations such as subjectivity, and low sensitivity. Video analysis technologies provides quantitative objective measures of gait,

where the subjective component is eliminated from data evaluation (the experimenter simply collects and analyzes the data) [40]. Furthermore, it is one of the few tests that allows a bridge between animal and human gait studies [28].

Most of the current video methods available for extracting gait features (for example the CatWalk in Figure 1.8 B) have not been able to fully capture quadrupedal locomotion, [49] partly because they were limited to stance event detection, (when paw touches the ground) compromising the full characterization of the gait cycle [50–53].

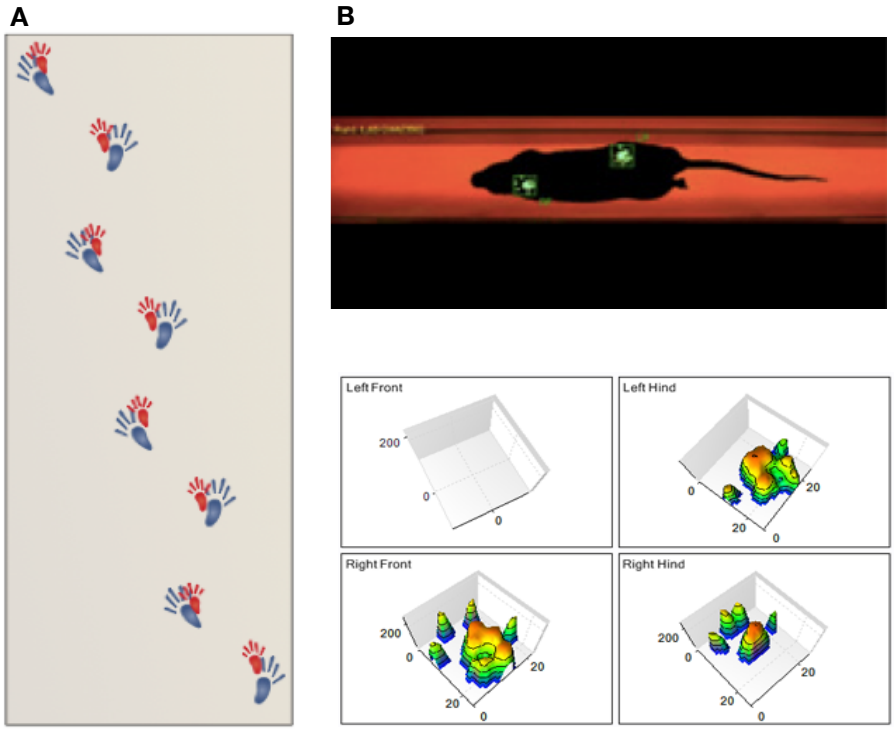

Figure 1.8: Gait analysis systems. **A)** Footprint test. The front and hind paw marks are left on the paper after the mouse walked on the absorbent paper. **B)** The CatWalk test uses the principle that underlies fiber-optics, fluorescent light illuminates the surface below the animal. At those planes where an object touches the ground, light escapes, only to be scattered by this object. Then, the place of contact becomes clearly visible and can then be quantified through movie analysis. Adapted from [28,51].

1.5.9.1 Locomouse setup

Capturing cerebellar-dependent coordination in mice is not an easy task. It requires a highly sensitive tool capable of quantifying coordination across the body that is evident when we observe a mouse walking [50].

Our lab previously developed a custom video tracking system (LocoMouse) for measuring and analyzing locomotor coordination during overground walking in mice. While the mouse freely crosses a 60 cm long corridor, a side and bottom view (using a mirror) is acquired at a high temporal resolution (Figure 1.9) [54].

To increase data acquisition, an automatic computer vision algorithm is used to track several mouse body parts without using surface markers. Hand labeled data is used to train linear Support Vector Machine (SVM) classifiers for each characteristic independently. The algorithm's output is a set of 3D coordinates: for each frame, the center of each of the four paws, the snout, and the tail divided in 15 segments are obtained (for more details see [54]). The LocoMouse Tracker code is available for download on GitHub (https://github.com/careylab/LocoMouse).

The LocoMouse setup provides an extensive quantification of locomotion kinematics by producing an extensive set of mouse gait parameters in three dimensions. Furthermore, this new analysis method for mouse locomotion already revealed fundamental features of gait cerebellar ataxia [54]. Importantly, it was demonstrated that basic stride parameters alone, although altered in an ataxic mice, do not capture the ataxic symptoms, and highlight the importance of accounting for walking speed and body size in data analysis [49,50,54–56].

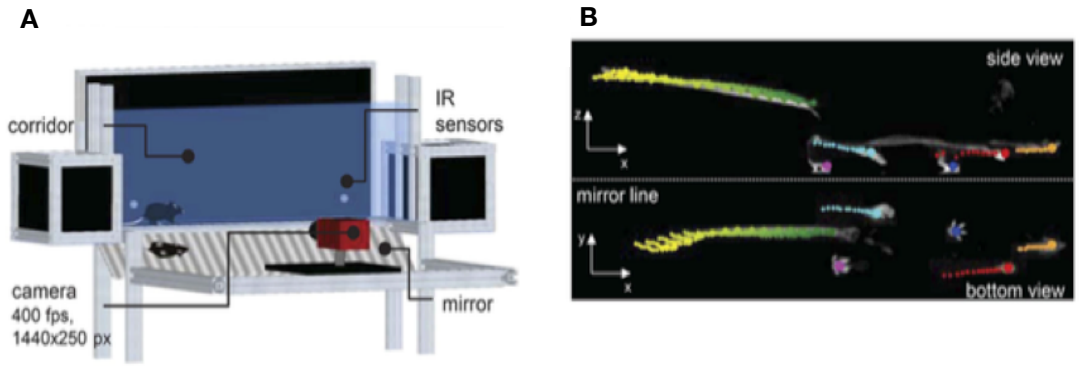

Figure 1.9: Locomouse setup. **A)** A high-speed camera records side and bottom views at 400 frames/second. Infrared (IR) sensors trigger data collection. **B)** A machine learning algorithm identifies paws, nose and tail segments and track their movements in 3D [54].

1.5.9.2 Treadmill

Another way to measure locomotion is to use high-resolution movie capture while the mouse is running on a treadmill [28]. These tasks have the advantage of manipulating the speed of the belts, which allows the measurement of the velocity modulation on gait parameters in a sensitively and accurately manner [33].

This paradigm has been used to study human locomotor adaptation. The motorized split-belt treadmill makes the independent limbs move at distinct speeds. Healthy humans can adapt to split-belt walking over time by changing spatial and temporal gait parameters. When the belts return to the same speed, (post-adaptation) controls show negative after-effects [4].

Within the lab we also implemented a split-belt treadmill walking task for the mouse. Using the LocoMouse video tracking system described previously it is possible to track body features in 3D. This represents an excellent assay to study motor adaptation in mice (Figure 1.10) (Darmohray et al., in preparation).

This type of motor learning is thought to involve the cerebellum, as previous studies have showed that patients with cerebellar lesions fail to adapt to the stimuli induced by the different belt speeds [57].

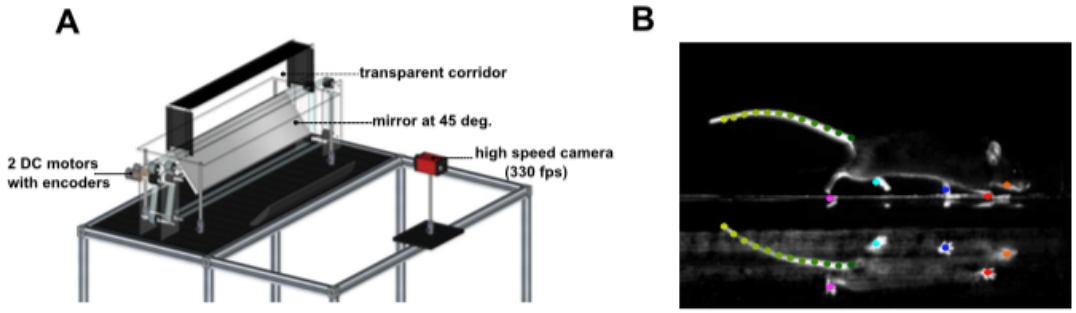

Figure 1.10: Split-belt treadmill for mice. **A)** The motorized split-belt treadmill forces the limbs to move at distinct speeds. **B)** The mouse body parts are obtained in 3D through video processing (Darmohray et al., in preparation).

1.5.10 Horizontal ladder

Horizontal ladders require the animal to precisely place its paws in a discrete way to successfully accomplish the task. This motor behavioral test sets accuracy constraints on the locomotive performance, as the animal has to step precisely on the rungs. In this relatively simple test, untrained mice spontaneously step throughout the ladder. Indeed, due to the common sequence of steps on the ladder, the mouse learns characteristic stepping patterns that enables the animal to predict rung positions and enhance motor performance throughout training [24].

The animal missteps are register in video acquisition, and are typically used as a measure of motor performance during walking [58–64]. In some studies, foot slip and foot-fault are distinguished by video inspection (Figure 1.11 A) [65,66]. Others give ordinal rating scores based on placement accuracy (typically the type of error made) [8,25,67–69]. This inspection analysis gives important details regarding whole-body functions, like postural adjustments and compensatory disabilities [68]. However, these qualitative measures are time-consuming and,

because they are normally designed for a particular type of deficit, they are not easily applied to other models [53].

This paradigm has successfully evaluated motor behavior within studies of rodent models for stroke, spinal cord injury and neurodegenerative diseases [69]. Moreover, this task has proved valuable to detect even subtle features of locomotor behavior, by being able to differentiate between compensation and pure motor function rehabilitation after motor system damage [24].

Furthermore, this technique is often associated with other tools, such as contact sensors coupled to the rungs to detect specific events of the locomotor cycle, [66] electromyography to record rodent's muscle activity [7,70] or is associated to other motor tasks, such as overground walking or as part of a combined test to evaluate general motor function [59,62,64,71,72].

The classical version of the test consists of a horizontal grid (Figure 1.11 B). However, several variants have been used. Test sensitivity can be increased by changing the spatial arrangement of the steps of the ladder [69,73–77]. In addition, these rung locations can also be changed throughout the experiment. These different arrangements induce new gait adaptations, which can be investigated in the context of learning during skilled walking [24,78].

The Erasmus Ladder can also be considered another variation of the ladder rung task [79]. This setup comprises a horizontal ladder in the middle of two black boxes. Each box has a light emitting diode (LED) and a compressed air outlet with the purpose of being used as triggers for initiating the trial (Figure 1.11 C). All rungs are coupled to sensors that detect touch events. This information can then be used to analyze the walking pattern of the mouse. Because it is possible to pair a barrier presentation with a specific tone, this system is also suitable to study locomotor adaptation [79].

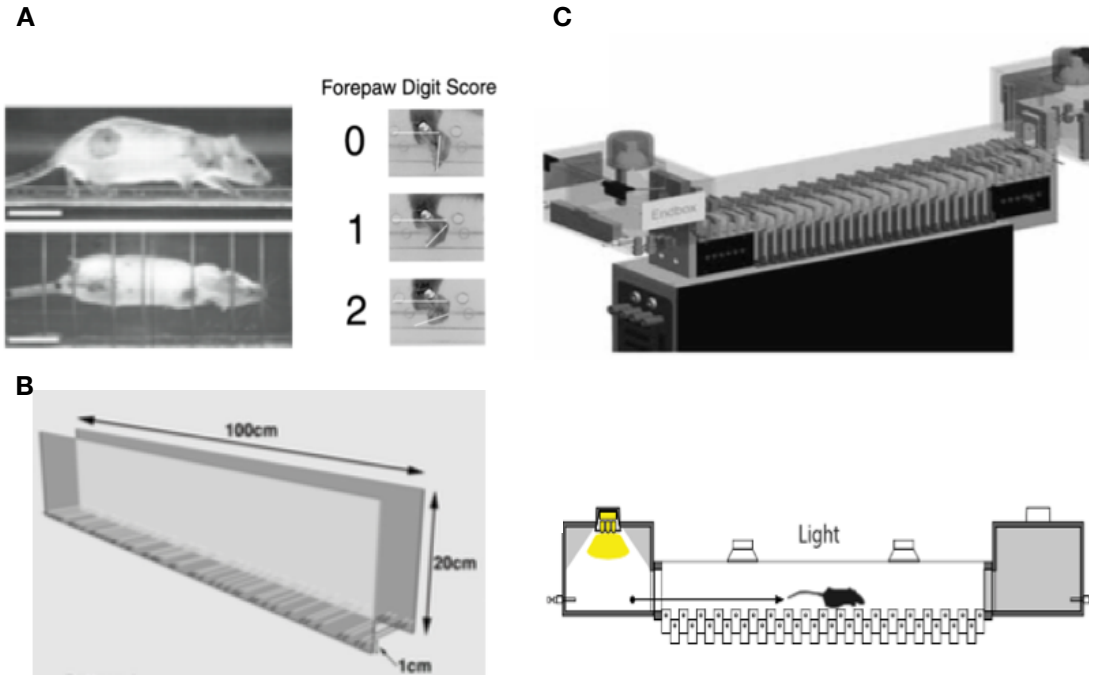

Figure 1.11: Examples of ladder paradigms. **A)** Example of paw placement rating score. **B)** Standard version of the ladder task. **C)** Erasmus ladder. In this example, light is used as a cue for departure. Adapted from [53,69,79,88].

Mechanisms built into the horizontal ladder task require the animal to adapt its normal walking by making either corrective movements following an unpredictable disturbance, or anticipatory modifications informed by sensory systems. To accurately accommodate the constraints forced by ladder, subtle alterations in limb trajectory and instantaneous changes in velocity and direction need to be precisely controlled. Thus, the ladder allows these fine-tuning aspects of motor control to be studied [73].

Moreover, some aspects of whole-body movements also need to be adapted. Studies in rats showed that, when compared to overground walking, the stepping behavior is much less variable, comprising significant changes in the overall posture. This suggests that this task requires a refined motor control, giving it unique features to reveal subtle impairments in locomotion that might not be apparent in assays like overground walking [46,80].

The ladder paradigms that exist to date are mostly limited to foot misplacements analysis that do not offer a quantified and sensitive examination of deficits related to the locomotor pattern [66]. Furthermore, most of the setups described are either limited to the time-consuming analysis of the movies recorded or do not provide information about step kinematics, which could be gained from automated tracking systems [25]. The Erasmus Ladder was able to quantify some aspects of interlimb coordination by analysis of the registered mouse contacts on the rungs of ataxic mice, [79] however the parameters provided might not reflect the main coordination problems observed in these mice [50].

The ladder paradigm is useful to measure the instantaneous locomotor changes while a mouse steps on the ladder, but also to access long term adaptations that might occur after several walking attempts (learning to walk on the ladder). Importantly, supraspinal structures seem to participate in both types of motor control [73,81,82].

Regarding locomotion control, studies in rats showed supraspinal structures involvement in controlling the accuracy of rhythmic limb movements while an animal stepped on a ladder [73,81,83]. Particularly, the cerebellum has been implicated in fine-tuning of limb coordination [84]. It can be hypothesized that performing intricate walking patterns involves the participation of motor cortex, basal ganglia and cerebellum. Together, these networks might generate appropriate commands that are sent to the spinal cord, that ultimately executes successful paw placements.

Furthermore, the cerebellum seems to be involved in learning of motor patterns in the ladder paradigm [82]. Cerebellar circuits might act by learning to plan motor actions in relation to repeated patterns of rung distribution [85].

Overall, the ladder paradigm described holds particular potential for studying the contributions of these supraspinal structures to both types of motor control.

1.6 Objectives

Based on the information gathered and discussed previously, we envisioned a motor behavioral paradigm that could provide an innovative and valuable approach to quantify locomotor coordination in a ladder configuration in mice.

This project aimed to **I)** build a new horizontal ladder paradigm, designated as *LocoLadder*, which had to meet the following requirements: **I.I)** the task should be fully automated through software control; **I.II)** the mouse should be able to freely step on the ladder without any restriction; **I.III)** allow assess to the vertical load modulation exerted by the paws by coupling force sensors to rungs of the ladder; **I.IV)** and record and track the mouse's body parts with high spatiotemporal resolution while the mouse steps on the ladder. Furthermore, we intended to **II)** use the developed system to quantifying locomotor deficiencies of a cerebellar ataxic mutant mice model.

At the same time, we wished to develop a flexible method that could be used to assess broad aspects of motor dysfunction.

1.7 Thesis structure

The present dissertation is divided into 4 chapters. The first chapter included a description of the underlying principles of motor function with particular focus on the role of the cerebellum in motor control. Moreover, the motor behavioral tasks for rodents were described along with the motivation purposes for this project. Finally, the main objectives and thesis structure were presented.

In the second chapter, it is highlighted the technical details of the *LocoLadder*, including the component parts, software and outputs. Additionally, in chapter 3, a behavioral experiment using the setup developed is described and discussed. The fourth and last chapter comprises an overall discussion of the thesis as well as all the conclusions gathered from this work. Finally, some limitations and considerations regarding future perspectives of this project are presented.

Chapter 2

The LocoLadder setup

The cerebellum is essential for an accurate and coordinated gait, however it is still a poorly understood component of the motor system. In spite of the fact that cerebellar dysfunction has been extensively characterized in humans and that we are closer to fully understanding simpler cerebellar-dependent behaviors in experimental animals, [3,18–20] we are still far from linking more complex whole-body movements to cerebellar circuit function. As motor behavior is the measurable output of the motor system, a better understanding of this system will certainly involve taking advantage of the current cutting-edge technologies to precisely quantify motor proprieties. The development of these tools together with genetic techniques to manipulate certain neurons might allow establishing causal relationships between neural circuits and specific aspects of behavior and ultimately gain deeper understanding of motor control.

Here we describe in detail the *LocoLadder*, which is a new ladder paradigm system to assess locomotor coordination in mice. This new system combines force sensor information with high-speed video capture with the goal of using both gait

analysis and load distribution profiles to sensitively and reliably quantify locomotor coordination in a ladder configuration task.

Our laboratory has already developed the LocoMouse, an apparatus to study locomotor coordination during overground walking [54]. The *LocoLadder* that is described below represents a modification of this system.

The setup consists of two black boxes connected by a ladder coupled with highly sensitive force sensors (Figure 2.1). Mice are filmed while they step through the illuminated ladder using a high-resolution video camera. Two infrared sensors located in the extremities of the corridor automatically trigger the start and stop of the data acquisition. A mirror placed below the corridor at an angle of ~45º allows simultaneous collection of side and bottom views in order to generate three-dimensional tracking data. All components are assembled within a movable aluminum frame structure to provide robustness and flexibility. Here, we will describe and characterize each feature of the *LocoLadder*.

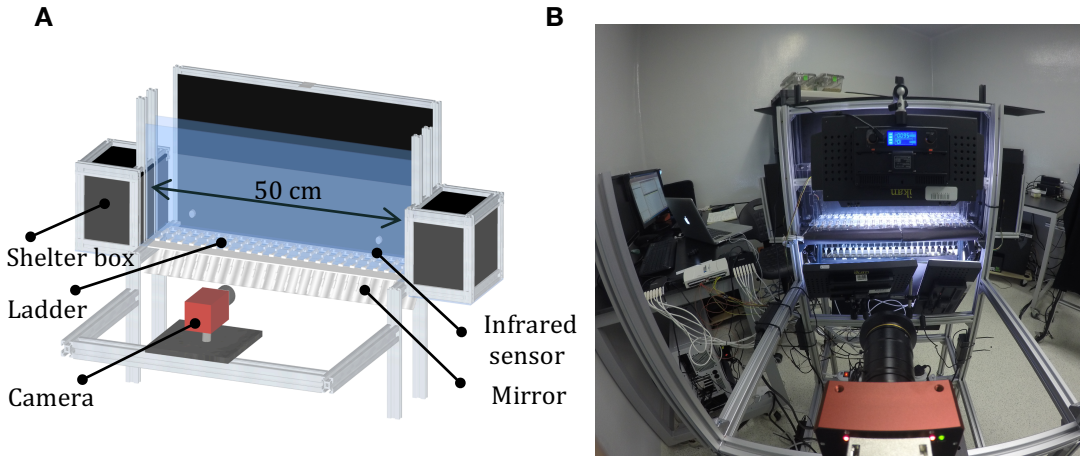

Figure 2.1: The *LocoLadder* setup. **A)** The principal components are represented in the model of the apparatus. **B)** Front view of the setup showing the light emitting diode (LED) array lights illuminating the top and bottom of the ladder.

2.1 Ladder

The overall design of the ladder is depicted in the figure (Figure 2.2 A). The 50 cm long ladder has 44 (22 on each side) rungs placed 25 mm apart from each other. Previous testing using several mice on overground walking revealed an average stride length distance around 50 mm with forepaw displacement, at medium velocity [54]. Thus, the use of 25 mm rung spacing provides comfortable walking for wildtype mice, which typically skip one rung in each stride and, at the same time, allows motor impaired mice to accomplish the task performing smaller (25 mm in length) strides. Furthermore, this ladder has a flexible rung arrangement, by changing the inter-step length and the number of rungs. A transparent 4 cm wide acrylic corridor constrains the mouse to walk in the center of the ladder (Figure 2.2 B). This configuration forces mice to place their paws on independent rungs, enabling single measures from the force sensors coupled to each rung. A transparent acrylic bottom is located at 1.5 cm below the ladder to prevent the mouse from escaping and to provide support when they miss the rungs.

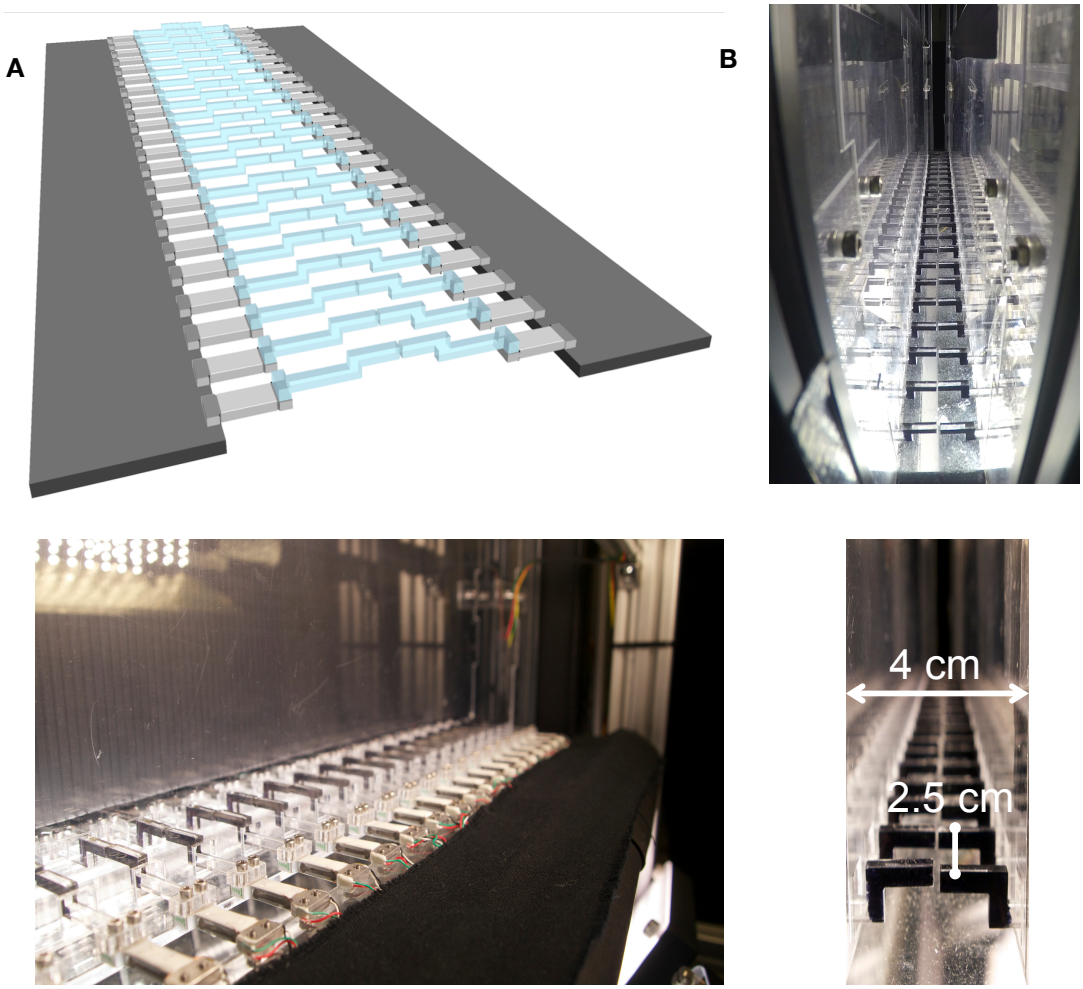

Figure 2.2: The ladder design. **A)** Model of the ladder (top). Acquisition boards (not shown) are meticulously located bellow the lateral ladder supports to provide side and bottom view video capture. **B)** Transparent acrylic corridor with 4 cm width. It is also highlighted the inter-step length of 2.5 cm. The ladder floor is also visible below the rungs.

2.2 Force sensors

The rungs (38 x 4 mm) are constructed with custom transparent acrylic components. The basic design is depicted in the figure (Figure 2.3 A). A mouse places its paws in the elevated part (18 mm width) to enable a better paw side-view capture for video recording. The side parts of the rung were painted black to minimize light reflection.

Each rung is connected to a single point load cell that measures forces in the vertical direction with range capacity of 100 g (model 3139, micro load cell,

Phidgets Inc.) (Figure 2.3 B). Two additional load cells are attached to the acrylic floor (15 cm from either end of the corridor) to detect misstep events.

These force sensors specifically detect the load applied in the vertical direction, ignoring the other types of forces. The place where the load is applied is not decisive because they are designed to measure a shearing effect on the beam, independently of the bending of the beam. Thus, this load cell gives precise outputs, independently of the load application point on the rung. These high-precision load cells use tiny strain gauge resistors to convert the force applied to an electrical signal. The gauges are encapsulated in a beam (within the white plastic in Figure 2.3 C). When load is applied, these strain gauges deform, provoking a resistance alteration in relation to the load applied.

The strain gauge output appears as the variable resistance that is detected by a bridge circuit as a voltage signal (Figure 2.3 C). The output voltage from the bridge is fed to an appropriate analog-digital converter (ADC) board, (PhidgetBridge, Phidgets, Inc.) (Figure 2.3 D) which amplifies the voltage signal. The amplified voltage signal is then converted to digital numeric values with a 24-bit resolution and fed to the computer through USB connection. Each ADC board connects to 4 load cells. We used 11 PhidgetBridges boards located bellow the ladder lateral supports to collect data from the 44 load cells.

Ratiometric mV/V measure is the output value in mV of the sensor, scaled for a 1V sensor supply voltage. This measure will match to the physical amount that the sensor is detecting, independently of the actual voltage provided to the sensor. After testing, we set the gain to 32 and a sampling interval of 8 ms for all force sensors (maximum data rate of the board). This configuration provides measurement interval in the operative sensitivity range (± 31.25 mV/V which encloses the 0.2 mV/V max measured while testing several mice on a ladder) and sufficient temporal resolution to detect mouse displacements. Moreover, a

resolution of 3.72 nV/V and rated output of 600 ± 150 uV/V is obtained with these load cells.

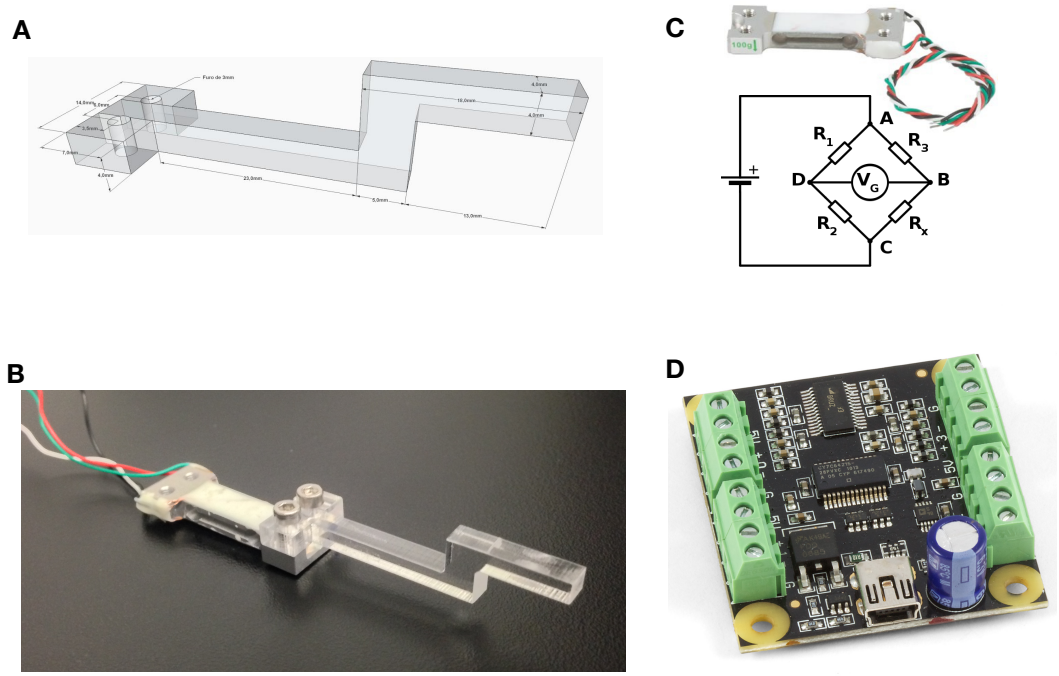

Figure 2.3: Sensing force elements. **A)** Custom designed acrylic rung. **B)** Applying force to one end creates stress in the bar, causing the strain gauge to deform. **C)** Micro-load cell. A Wheatstone bridge circuit is the generic method to measure the resistance in the strain gauges. **D)** PhidgetBridge board collects data from 4 load cells simultaneously.

2.2.1 Calibration procedure

Calibration is performed on each 44 load cell to calculate the relationship between the load and digital readings for each load cell, obtaining weight values from the digital intensity values outputs of the sensors. To do so, we put two calibration weights of 1 g and 20 g, (previously measured in a high precision weighing device: 0.9892 g and 19.9823 g, respectively) one at a time, on the individual load cell. These weights were chosen based on typical load range exerted by mice on previous testing. With the weight in place, we collected 1000 samples from the ADC converter and registered the median value of the two

weights. Indeed, the intensity value with the load cell unloaded is registered. Thus, the relationship between 3 different loads (0,1 and 20 g) and their corresponding readings are obtained. Then, we use the values to make a linear equation that converts the PhidgetBridge output in mV/V (X) to grams (Y). The two calibration parameters (a,b) determine the slope and offset for the calibration: (Y = aX + b) (Figure 2.4). The procedure is repeated and the calibration coefficients are registered for each load cell. To minimize this time-consuming procedure, a custom-written LabView code was developed to automatize the data registering and median value computation.

On the experiment described in chapter 3, calibration was performed before the start of session one. The offset load values slightly changed throughout the days, condition intrinsic to load cells called creep effect (we measured < 1 g change for all 44 load cells at the end of session 5). To account for this, several measures were registered throughout the experiment. Before the beginning of each mouse session, the offset change for all load cells was registered for further subtraction to the offset measured in day 1.

Furthermore, we have to keep in mind that, ideally, the output of the sensor is perfectly linear, and a simple 3-point calibration should exactly describe the behavior of the sensor at other loads. In practice, the sensor is not perfect, and these sensors have an intrinsic non-linearity maximum error of 50 mg, that describes the maximum deviation from the linear curve. Theoretically, if a more complex calibration is used, some of the non-linearity can be factored out, but this would require a time-consuming calibration with multiple points.

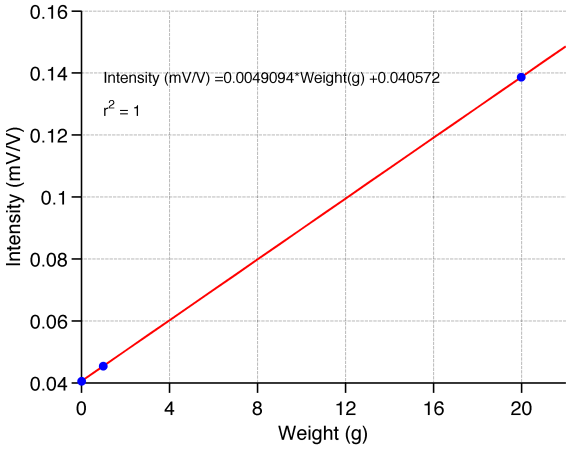

Figure 2.4: Calibration curve. With the formula obtained we can easily convert intensity to weight values. A correlation coefficient of 1 was obtained in this example.

2.3 Camera

A high-resolution (2320x1726 pixels) and high-speed camera (Model Bonito CL-400B, Allied Technologies) was used to record a side and bottom view with the help of a mirror placed at ~45 degrees under the ladder (Figure 2.5 A). An installed frame grabber enables the interface between the camera and the computer (PCIe-1433 bus, National Instruments).

2.4 Boxes and IR sensors

Each shelter box is a black vinyl box with a removable opening on one of the sides to easily handle the mouse. The box has a small doorway that provides free access to the ladder. These boxes have infrared (IR) sensors inside to detect the presence of the mouse (Figure 2.5 B, in blue). Mice freely trigger and terminate the trial acquisition (camera and load sensors) by freely passing through 2 extra IR sensors located in the beginning and ending of the corridor (2.5 cm from either end of the corridor). The infrared sensors are connected to a data acquisition (DAQ) measurement system, (USB-6211, National Instruments) which connects to the computer through USB connection.

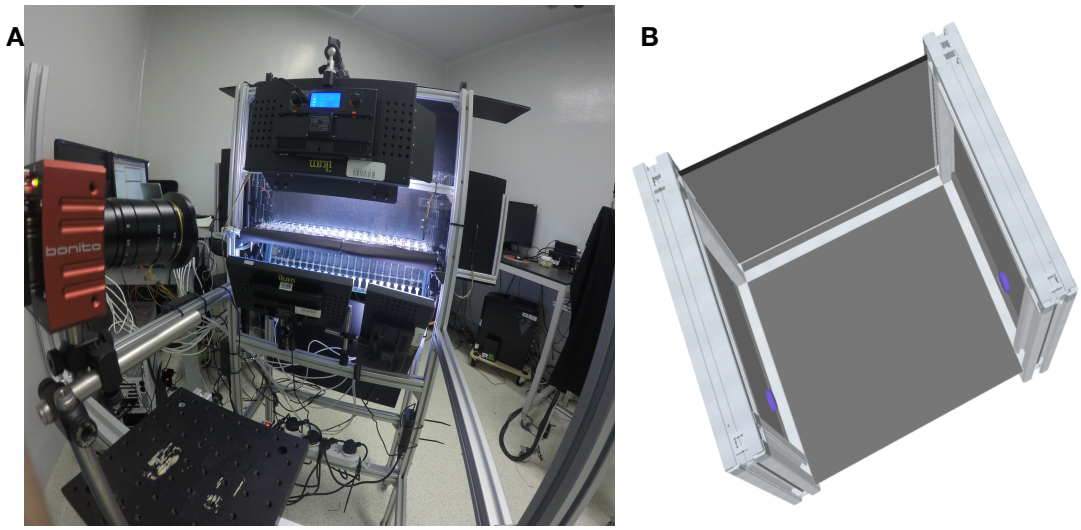

Figure 2.5: Camera and shelter boxes. **A)** A Bonito CL-400B camera records the side and bottom view. **B)** IR sensors (in blue) located within the black boxes detect presence of the mouse.

2.5 Software

The *LocoLadder* is controlled by custom-written LabView code and uses Phidgets ADC Bridge boards and National Instruments PCIe 1433 and USB-6211 to record and save the movies in real time. The machine itself is an Intel Core i7-4790 CPU 3.60 GHz and 32 GB of RAM running windows 8.1 pro operating system.

The figure depicts a basic flow schematic of the program (Figure 2.6 A). First, after the mouse's weight is obtained, subject information (ID, weight, condition, age, session and number of runs) is typed by the experimenter on the interface (Figure 2.6 B) which will provide an identifier name to the data file. Then, the experiment runs the program and, before the mouse session starts, a background image is captured and the median values of each unloaded 44 load cell is registered for further background subtraction and sensor calibration process. Also, an error check conditions, evaluates if the load cells are reading reliable

measures and informs if everything is working reliably before starting. After this, the program is ready to start and the experimenter places the mouse inside of one of the shelter boxes.

An infrared sensor detects when a mouse enters the corridor and triggers data acquisition. The camera and load sensor acquisition occur in two independent loops and at two different data rates (500 frames/second and 125 samples/second, respectively). Thus, they are not synchronized in time. Both types of data collection are automatically saved to two independent text files (camera saved as a binary file to minimize processing time). When mice reach the other IR sensor, the acquisition stops. The program discards the trial if the mouse returned to the initial shelter box (by reaching the IR previously activated). This sequence is repeated for the predefined number of valid runs. Once the trial number goal is reached, the system is closed and the movie binary files are converted to avi movie format. A set of 3D coordinates of the mouse features of interest are obtained from the movies by applying a previously developed tracking algorithm [54]. The software was written in Matlab (Mathworks). The LocoMouse Tracker code is available for download on GitHub (https://github.com/careylab/LocoMouse).

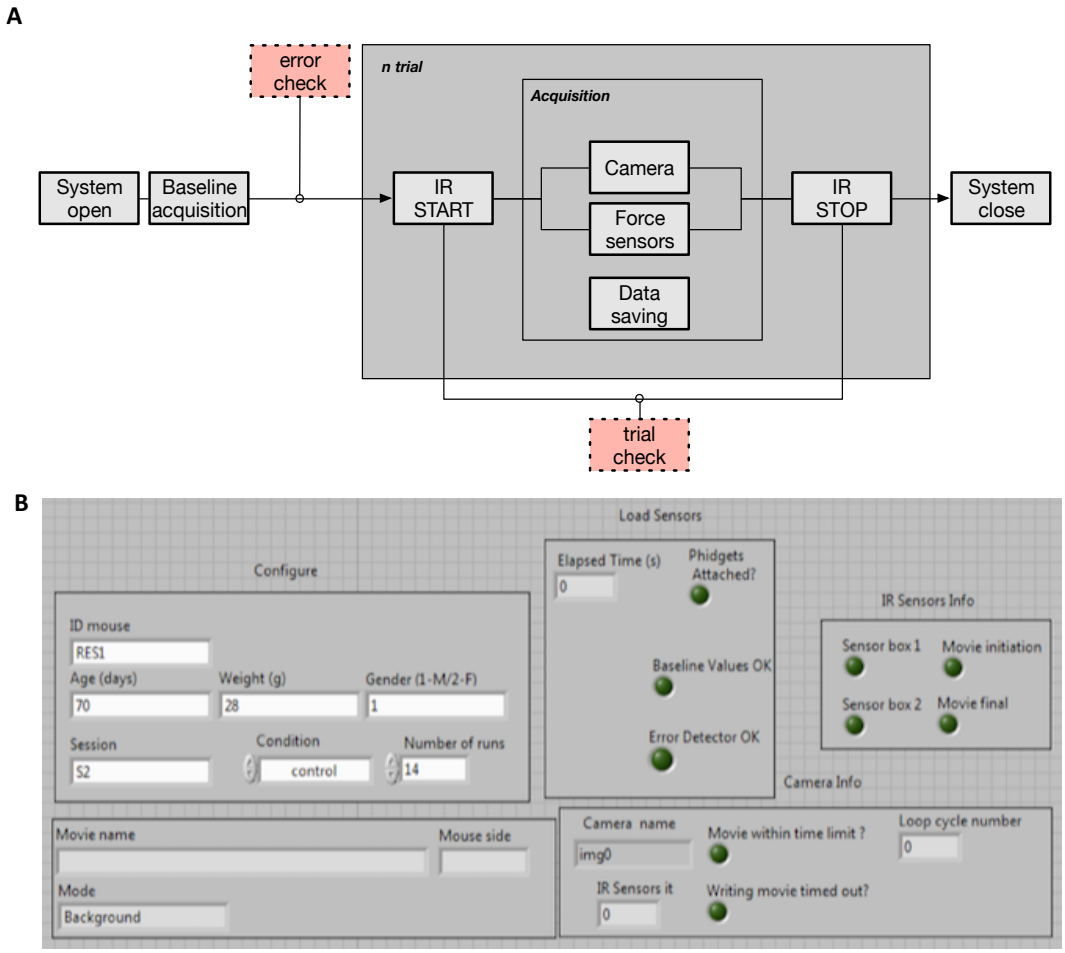

Figure 2.6: Software control. **A)** Basic program flow. Before each session, a baseline acquisition and force sensor check is performed. Between acquisitions, the program checks the validity of the trial. **B)** Interface layout. Here the experimenter registers mouse information and obtain information on ladder status.

2.6 Data output

The *LocoLadder* provides detailed information about each mouse passage along the corridor (Figure 2.7). The force sensors extract the load profile exerted on each individual sensor during the trial **(see example trial – Movie 2.1)**. Using sensor activation detection algorithm (described in Appendix I) we obtain the activation period of each sensor (as shown in Figure 2.7 B, superimposed on the paw x trajectories). At the same time, the machine learning algorithm detects and tracks all four paws, snout, and 15 tail segments in both bottom and side

views for each trial. We then extract the continuous forward (x), side-to-side (y), and vertical (z) trajectories for each feature. **(see example trial – Movie 2.2).** Within the lab, we have already developed an algorithm to detect the different phases of the stride cycle based on the forward trajectory obtained from the tracking (for more details see [54]). Using this tool we can extract the swing (paw leaves ground) and stance (paw touch down) onsets of each paw (as demonstrated in Figure 2.7 E, superimposed on the load activation period of the left and right sensors).

Misstep detection and body mass center computation were also obtained. Misstep detection used the load information from the two sensors embedded on the floor below the ladder (see Appendix II for details on the computation). Body mass center was obtained through application of image processing techniques applied on the video acquired (see Appendix III for details on the computation).

In chapter 3, we describe an experiment using the *LocoLadder* setup capabilities to quantify the locomotor profiles of both wildtype and cerebellar ataxic reeler mice.

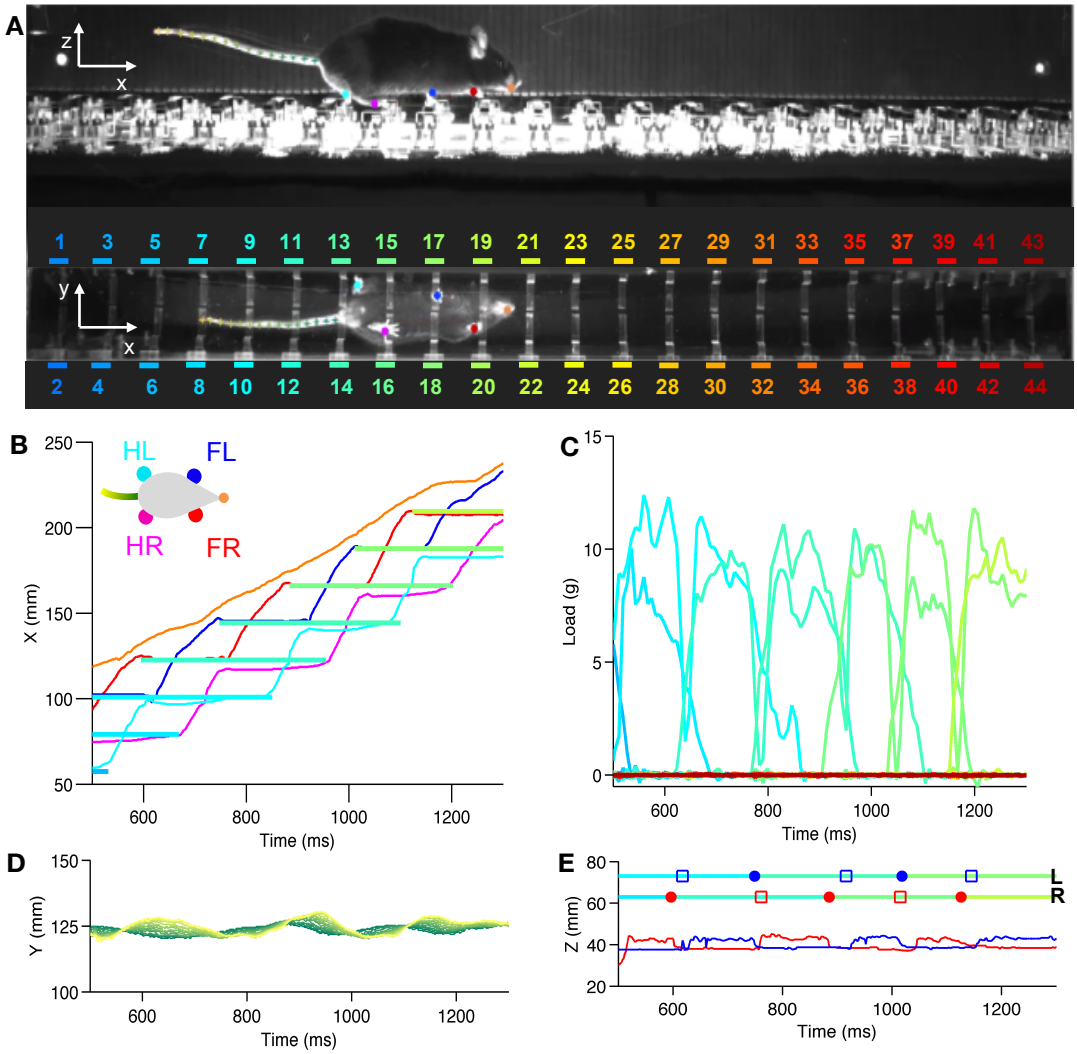

Figure 2.7: *LocoLadder* output data. **A)** Mouse crossing the ladder. Each paw, tail, and nose are identified by the LocoMouse automated tracking system. Continuous tracks are obtained by post-processing the feature detections with a computer vision algorithm. **B)** Continuous forward trajectories (x position versus time) for nose and paws. Each sensor activation period is superimposed on the limb x trajectories. Sensor data is color coded according to the numeration above**.** The drawing illustrates the color code used to identify individual mouse features. **C)** Load exerted on each force sensor. **D)** Side-to-side (y) position of proximal (green) to distal (yellow) tail segments versus time. **E)** Z position combined with load information and swing and stance points. Below it is shown the continuous vertical (z) trajectories of the two front paws. On top, it is represented the left and right activation periods of each sensor. The swing and stance events for the front (red) and right (blue) paw are superimposed on the load activation traces. Solid circle – stance onset; Open square – swing onset.

Finally, it was developed a user interface (GUI developed in Matlab) to easily upload data from an individual trial and explore both the movie and load sensor data (Figure 2.8 A). We can easily identify the swing and stance events of a mouse stride cycle while exploring the raw data provided by the ladder apparatus (Figure 2.8 B).

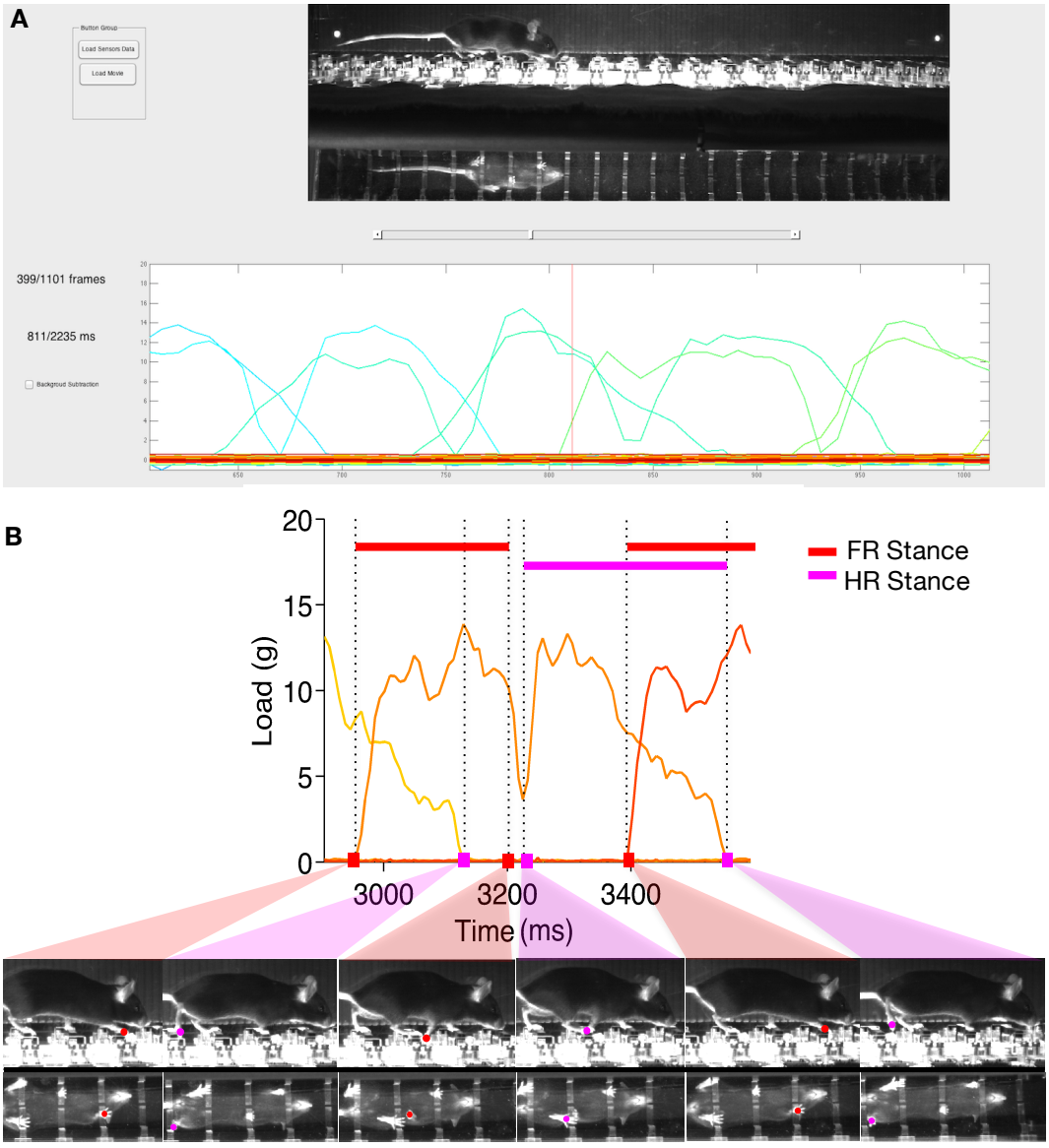

Figure 2.8: Data exploration. **A)** GUI interface layout for data exploration. **B)** Load data highlighting swing and stance onset events of right paws. Below are shown the corresponding sequence of side and bottom view images. Red and purple color coding for front and hind right paw, respectively.

Chapter 3

Quantifying locomotor deficiencies of reeler mice

In the previous chapter, a detailed technical overview of the *LocoLadder setup* was described. In the present chapter, we describe a behavioral experiment using the setup developed. We aim to provide evidence of some of its strengths in quantifying several relevant aspect of locomotion of a specific cerebellar mutant mouse model. Finally, the results obtained are discussed.

3.1 Reeler mutant mice

Distinct cerebellar mutants, which show abnormal cell configuration, have been characterized according to their gait [15,21–23]. These mice exhibit cerebellar ataxia and motor coordination deficits and have been used to study cellular processes, in addition to help create novel methods to treat these disorders [15,21].

In the study described in this chapter, we used reeler mutant mice model. Reeler mice exhibit an autosomal recessive mutation on chromosome 5. The specific gene is responsible for encoding an important extracellular matrix protein called reelin, which is specifically important in crucial phases of development [15]. The homozygous reeler mouse presents a generalized cellular disorganization across the brain, which affects not only in cerebellum but also in neocortex, inferior olive, olfactory bulb, cochlear nucleus, superior colliculus and substantia nigra [15].

The cerebellum is the most affected brain region. The overall structure is smaller and the characteristic foliation is no longer present. The circuit is also altered; granule cells and Purkinje cells are significantly reduced [15].

Reeler mice exhibit an interesting behavioral phenotype. They present striking uncoordinated and unstable walking, lack of balance, motor impulsivity and tremors [86,87]. By comparing them to non-ataxic controls, including heterozygous and wildtype, homozygotes show reduced balance on the beam walking and rotarod tests [15,21]. Moreover, mutants exhibited deficiencies in visuomotor guidance and spatial learning assays [15].

3.2 Methods

3.2.1 Apparatus and behavioral protocol

Experiments were executed using 20 mice divided in two groups: (a) Littermate controls comprised heterozygous (N=2) and wildtype (N=12) (n=1241; N=14 mice; 5 males; 9 females; 13-30 g, 48–78 days old) and (b) homozygous reeler mice (n=494; N=6 mice; 4 females, 2 males; 13–19 g, 49-73 days old) (Figure 3.1).

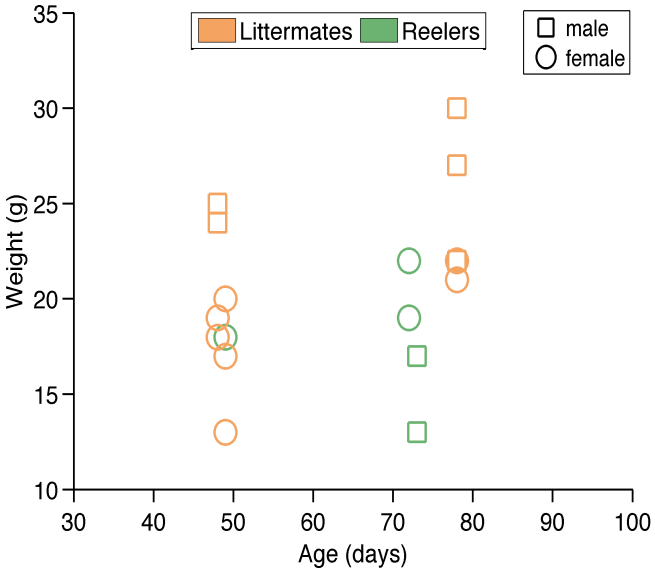

Figure 3.1: Mouse information. Weight and age for each experimental group are shown. The measures showed here were registered in the first session of each mouse. Reelers – green; littermates – orange. Circle – female; square – male.

All procedures were in accordance with the Champalimaud Centre for the Unknown Ethics Committee guidelines, and approved by the Portuguese Direccção Geral de Veterinária (Ref. No. 0421/000/000/2015). These mice were maintained in institutional standard cages with access to water and food. No invasive manipulations were performed in mice.

Mice freely entered the corridor, stepped across the ladder and self-initiated the trials by passing through the IR sensors. This was important for reducing stress and enhancing data acquisition. No kind of restriction or reward was used. Each mouse had to perform one daily session during 5 days. This was the first time they were exposed to the apparatus. Before each session, mouse information, including name weight, genotype and gender were registered before the mouse was placed in one of the boxes. Each daily session consisted of 15 to 20 trials during which the mouse had to freely walk back and forth on the ladder. When a mouse initiated the trial, video and force sensor data were acquired as previously described in Section 2.5. Trials with durations longer than 30 seconds and trials in which mice turned around and returned to the original box were not

saved. These trials largely reflected exploration behavior, which was not our particular interest. Mice did not show any sign of avoidance behavior, as they freely left the black boxes and cross the ladder at their will.

3.2.2 Data processing and analysis

Mice body tracks were obtained using a previously developed LocoMouse Tracker video-processing system (for more details about the algorithm see [54]). Afterward, tracking and force sensor data were analyzed using a custom-written code in Matlab.

Paw touch events on each rung and on the floor of the ladder were extracted using a custom-developed algorithm combining force sensor and tracking data (see Appendix I). To evaluate mouse locomotion several locomotor parameters were computed as follows:

Trial duration - time in milliseconds to travel between the two infrared sensors localized in the extremities of the corridor (see Section 2.4 for more details on the IR sensors).

Stride length - distance in centimeters between two consecutive touches on the same side of the ladder and on non-repetitive rungs. Thus, x displacement from touchdown to touchdown of front right and front left paw were obtained. For trial-wise analysis, the mean front-right stride length was used.

Missteps – number of touches on the floor located at 1.5 cm below the ladder during each trial (misstep detection is described in Appendix II).

Number of rungs used – number of unique rungs touched within a trial.

Contacts per rung – number of touches on each rung. For trial-wise analysis, the mean number of touches on each rung across a trial was computed.

Total contact time – time duration between the first and last contact on an individual rung (Figure 3.4 A). For trial-wise analysis, the mean duration of total contact times across a trial were computed.

Partial contact time - time duration of each contact on an individual rung.

Coefficient of variation - To evaluate the variability of whole-body oscillations, the coefficient of variation $\left(CV = \frac{\sigma}{\mu}\right)$ of the y position of the body was computed for each trial (see body mass center computation details in Appendix III).

Impulse - in order to evaluate the amplitude of the load profiles in both mouse groups, the impulse $(Imp = \int g\, dt)$ was calculated, being equivalent to the area below the load profile curve. The values were then normalized by the mouse's weight. The average of the normalized impulse was then obtained for each speed bin (0.05 m/s bin width).

F-measure – we performed a classification analysis using the frequency profiles of the load data. To do this, we used a pruned C4.5 decision tree (confidence factor: 0.25; cross-validation: 10 folds). Data was divided into 6 speed bins (0.1 m/s bin widths) and the same number of instances per class, (reeler/littermate) per bin were selected. Classification accuracy was assessed using F-measure $\left(F = 2\times\frac{precision\,.\,recall}{precision+recall}\right)$. This classification analysis was performed using WEKA data mining software (University of Waikato, New Zealand).

To statistically analyze the modulation of walking speed on several locomotor parameters between mouse groups we grouped our data by individual animals (as performed in [54]). All data was sorted into trial duration bins, (2 s bin width) with a minimum of 5 trial counts per animal per bin.

For the walking pattern analysis, a correlation matrix was calculated for the load sensor data. This matrix gave the correlation coefficients between all permutations of 2 sensors (for the total 44) across a trial. Indeed, for each trial,

correlations coefficients >0.35 were quantified and categorized according to the rung spatial arrangement. Due to the matrix symmetry, only half diagonal matrix was considered.

The ground reaction forces signatures were analyzed using all load profiles of each paw-rung contact. The load signal was normalized for the paw-rung contact period and the force amplitude was divided by the animal's weight measured in that session. For each load profile, average walking speed was calculated dividing the forward motion of the body center during the contact period. All data was sorted into speed bin, (0.05 m/s bin width) with a minimum count of 200 per bin.

Tracking data was used to analyze stride event onsets in littermates. In order to obtain the events of the gait cycle associated with each load profile, we used a previously developed algorithm, (see details in [54]) that extracts the swing and stance points and the corresponding x values for all four paws. For each activated rung, we selected the swing and stance points that had corresponding x locations near that rung. Then, the left or right swing and stance points were chosen based on the rung side (selected right front and hind paw events for a right activated rung and the opposite for a left rung). Finally, the time onset of the selected points was normalized to paw-rung contact period.

For each event type, (front stance, front swing, hind stance or hind swing) the data was then quantified in several percentages bins (%) of paw-rung contact (5 % bin width) and velocity (0.05 m/s bin width) bins. The median value was also computed for each speed bin. We used the overall center of the data because the data showed outlying measurements, specially at low speeds.

To investigate the presence of tremor, a time-frequency energy spectrum analysis using a Morlet wavelet method (sampling frequency: 62.5 Hz; cycles in wavelet: 100) was used (for more details, see Appendix IV). A frequency

distribution for each load profile was obtained and, as the ground reaction forces, all data was sorted into speed bins, (0.05 m/s bin width) with a minimum count of 200 per bin.

3.2.3 Statistical analysis

The statistical analysis was performed in Matlab. Linear mixed effects models were used to characterize and statistically compare the data acquired. Because our data comprised varying number of measurements per animal and data points per speed bin these techniques were chosen. All models were random intercepts, including the parameter measured (response variable) as a function of the fixed-effects (genotype and trial duration) and a random-effect term (individual animal). The resulting models obtained from the linear-mixed effects method are showed on Figure 3.6.2. Results are presented as conditional F-tests. Differences were considered statistically significant when the calculated p-value was <0.05.

3.3 Results

While observing reeler and littermate mice walking on the ladder, it was clear that they stepped differently. While reeler mice struggled to accomplish the task, control littermates crossed the ladder almost effortlessly **(see representative movie trial for both reeler and littermate – Movie 3.1).**

By visualizing the load raw profiles within a representative trial of both mouse groups we observed marked differences. The load profiles of each 44 sensors (with weight values represented in colormap gradient) during the trial are represented for both groups in Figure 3.2. While control littermate displayed smooth load gradient transitions, reeler mouse showed random sharp load transition with no clear pattern between left and right limbs (zoomed in Figure

3.2). Furthermore, contrary to the reeler mouse, a clear pattern of the weight distribution of higher loads correspondent to stance phase (paw touch down) of the diagonal paws support was usually observed in the littermate trial.

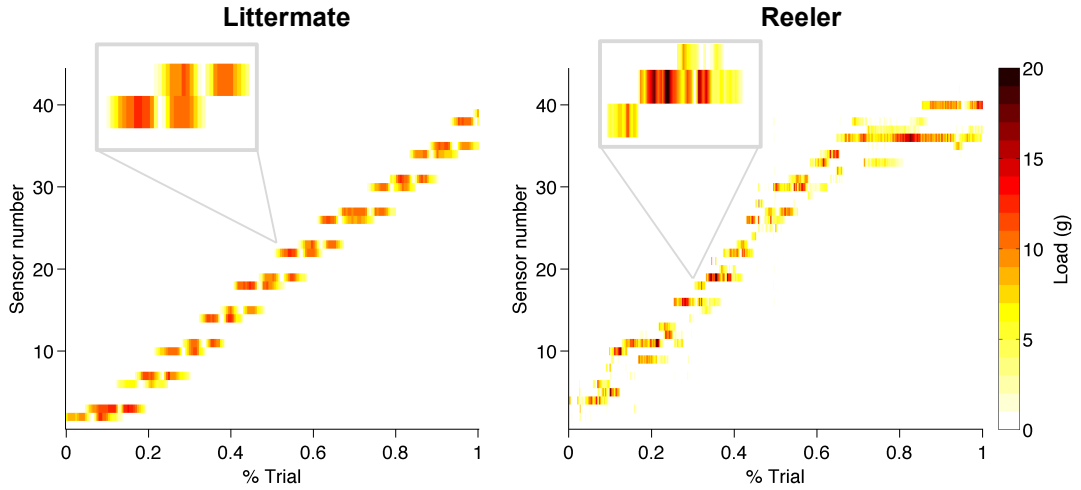

Figure 3.2: Load profiles during a trial for each mouse type. Each horizontal line in the plot (y-axis) represents the load profile of a single sensor. Load values between 0-20 g are shown in a color gradient.

3.3.1 Overall locomotion

Basic locomotor parameters

In order to further investigate how these two mouse groups behaved differently, we quantified and analyzed several basic locomotor parameters. Parameters such as trial duration (s), stride length (mm), missteps and number of unique rungs touched by the mouse paws were measured for each trial (Figure 3.3. Reelers in green and littermates in orange).

The trial duration for both groups was highly variable (Figure 3.3 A). However, reeler mice exhibited longer duration trials, as reeler histogram is shifted towards longer durations when compared to littermates. The mean values of stride length, missteps, and number of rungs used across the 5 sessions for each animal are shown (each subject represented by each line) (Figure 3.3 B, C and D). All parameters showed a clear distinction between the ataxic and non-ataxic mice. Reeler mice exhibited shorter strides, higher stepping errors and more rungs

used. Strikingly, reeler mice touched on almost double the number of steps in order to finish the task. Control littermates showed high variability in stride length and in number of rungs used. Individual reelers exhibited variable misstep counts within their group and an unclear global trend throughout the sessions. The remaining parameters were relatively constant across sessions for all animals, suggesting no learning component throughout the sessions. In summary, when compared reelers to controls, the clear distinction in the parameters computed reflected the low efficacy and stepping accuracy of their walking on the ladder.

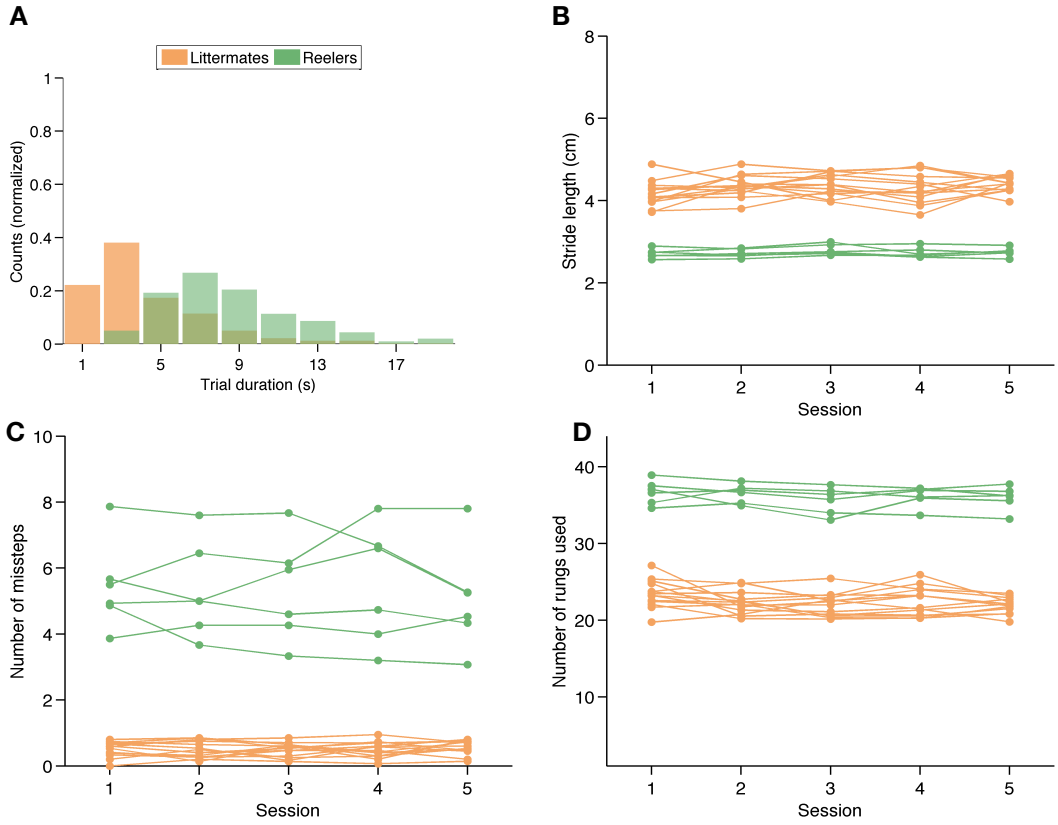

Figure 3.3: Basic locomotor parameters. **A)** Trial duration histogram (2 s bin width). Counts are normalized in each group. **B)** Stride length for the front right paw. Each line represents a different animal and each dot represents the mean value of the parameter within a session. **C)** Number of missteps. **D)** Number of rungs used. Reelers are shown in green and littermates in orange. For further detail on parameter computation, see Section 3.2.2.

Paw-rung contact

Relevant details of locomotor function can be revealed by analyzing how a mouse interacts with each rung of the ladder. When a healthy mouse is passing across a particular rung, it will typically extend and direct one of its front limbs to the rung. After the front paw is correctly placed and is stably on top of the rung, the hind limb of the same side will follow the front limb. Ultimately, the front and hind paw meet on the same rung before the front paw takes off. We hypothesized that in a motor impaired mouse this mechanism would be changed. Specifically, the paw placement on the rung and the timing associated with the paw-rung contact might be altered.

We recorded and analyzed several parameters that assessed how all four limbs interacted with each individual rung on the ladder. The number of contacts per rung, total contact time (ms) and partial contact time (ms) were quantified. The time duration between the first and last contact and the duration of each unitary contact were computed as total and partial contact time, respectively (Figure 3.4 A). The mean contacts per rung for each individual animal across sessions are shown (Figure 3.4 B). Reeler mice exhibited variable but higher number of contacts per rung when compared to control littermates. Total partial contact time histogram showed higher variability in reeler mice, contrasting with littermates that showed durations mostly within 100-400 ms. Moreover, most reeler partial contact times fell within a lower range (0-200 ms) when compared with control littermates (mostly between 100-300 ms). The low partial contact times in reeler together with their increased latency to cross the ladder suggests that the higher contacts per rung reflected multiple touches carried by the same paw.

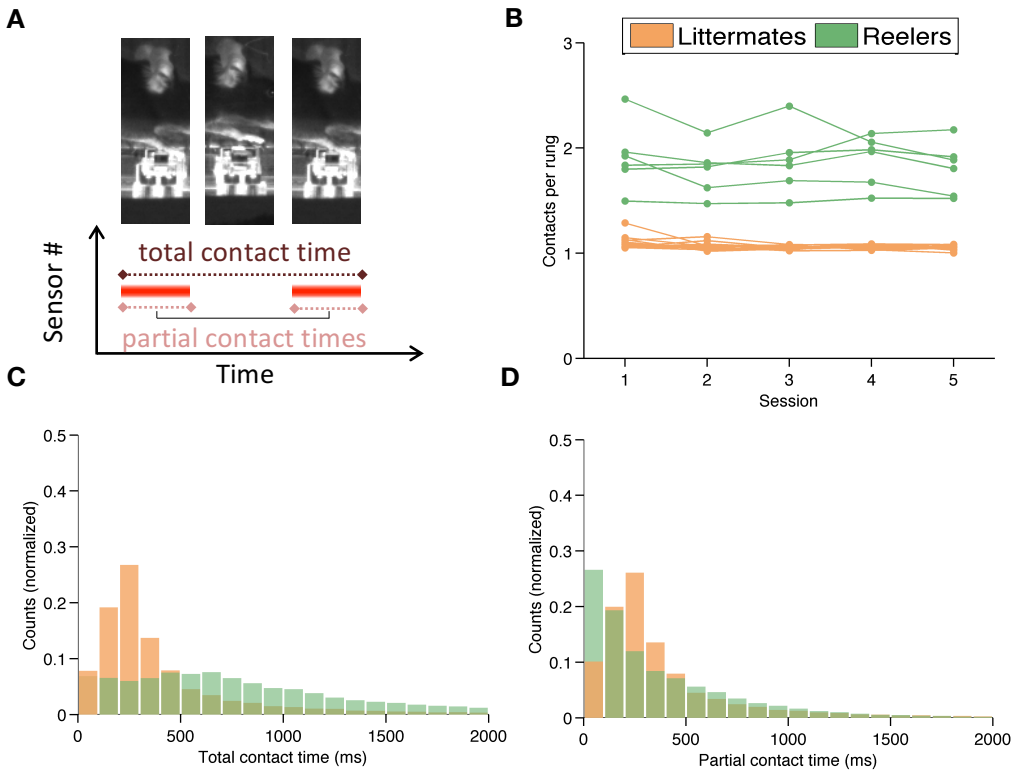

Figure 3.4: Paw-rung contact analysis. **A)** An example of total and partial contact time of a double touch in an arbitrary rung. The two red lines represent two separate touches. **B)** Contacts per rung. Each line represents a different animal and each dot represents the mean value of the parameter within the session. **C, D)** Total and partial contact time histograms, respectively (100 ms bin width). Counts are normalized for each group.

PCA analysis

Next, we were interested in understanding how the parameters computed previously individually contributed to the distinct locomotor behavior observed between the two mouse groups. After normalization, principal component analysis was performed using all the above parameters (trial duration, missteps, mean stride length, number of rungs used, mean contacts per rung and mean total and partial duration). Two principal components showed a clear separation between two clusters that match with the two mouse groups (shown in the two distinct colors in Figure 3.5). The locomotor parameters exhibited different correlations with each principal component, as shown by the eigenvalues in the table (Table

3.1). The second component is strongly correlated with number of rungs used and missteps, whereas the first component primarily correlates with trial duration. In addition to the clear clustering separation using basic locomotor parameters, these 3 measurements were the most distinct parameters between the two mouse groups.

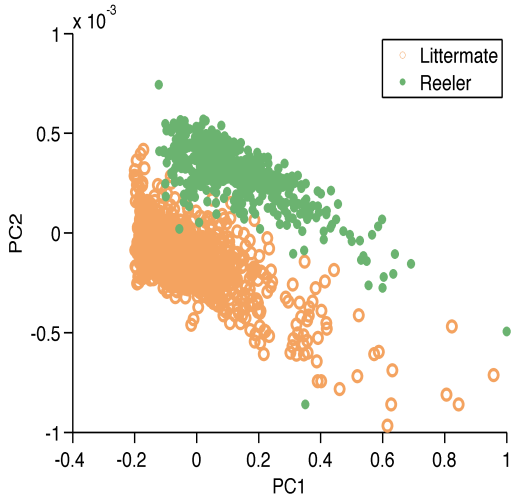

Figure 3.5: PCA analysis. Each marker represents a trial characterized by the 7 parameters previously computed. The first two principal components represented 99.8 % of the data.

	PC1	PC2
Trial duration	1.0000	-0.0021
Nr rungs used	0.0011	0.9506
Missteps	0.0004	0.2841
Contacts per rung	0.0001	0.0423
Total contact time	0.0001	0.0021
Partial contact time	0.0000	-0.0152
Stride length	-0.0001	-0.1164

Table 3.1: Eigenvalues obtained for the parameters measured.

3.3.2 Effects of walking speed on ladder walking

Previous studies showed that mouse locomotor parameters are dramatically influenced by walking speed [49,50,54–56]. Therefore, in this section, we analyzed how walking speed modulated the computed locomotor measurements. We used trial duration as a proxy of mouse's walking speed. The parameters missteps, mean stride length, number of rungs used, mean contacts per rung and mean total and partial duration are shown as a function of trial duration (Figure 3.6.1).

All parameters showed modulation across different trial durations. The number of missteps is positively modulated by increasing trial duration in reelers but not

in non-ataxic mice. Control littermates demonstrated 0 to 3 missteps across all trial durations (Figure 3.6.1 A). In general, there were higher contacts per rungs and partial contact time with increased trial duration, however the effect was strikingly different between the two mice groups. Reelers exhibited stronger linear modulation of trial duration on contacts per rung when compared to littermates (Contacts per rung: $F(66.51,1) = 109.96$; $p<0.05$. See fitted lines in Figure 3.6.2 obtained from the linear mixed effects models). On the other hand, ataxic mice showed a lower effect on the partial contact time (Partial contact time: $F(66.88,1) = 73.18$; $p<0.05$). Stride length generally tended to decrease, while number of rungs used increased with longer trial duration in both groups. However, they were differently modulated by trial duration in the two groups of mice (Stride length: $F(74.85,1) = 25.34$; $p<0.05$; Number of rungs used: $F(69.89,1) = 8.49$; $p<0.05$). In both parameters, littermates displayed high variability in the data (Figure 3.6.1 B and C). Total rung contact time was strongly influenced by trial duration, nonetheless they were surprisingly not significantly different between groups (Total contact time: $F(67.28,1) = 0.18$; $p = 0.68$. See Figure 3.6.2 E). All together, we observed that all locomotor parameters were influenced by trial duration, suggesting the effect of walking speed on these parameters. Moreover, they were differently modulated in both mouse groups, except for the total contact time. Despite the higher variability observed in reeler mice, (Figure 3.4 C) when considered the effect of walking speed, the total contact duration was not significantly different between the two groups, (Figure 3.6.2 E) and was also not revealed by the PCA analysis (Table 3.1).

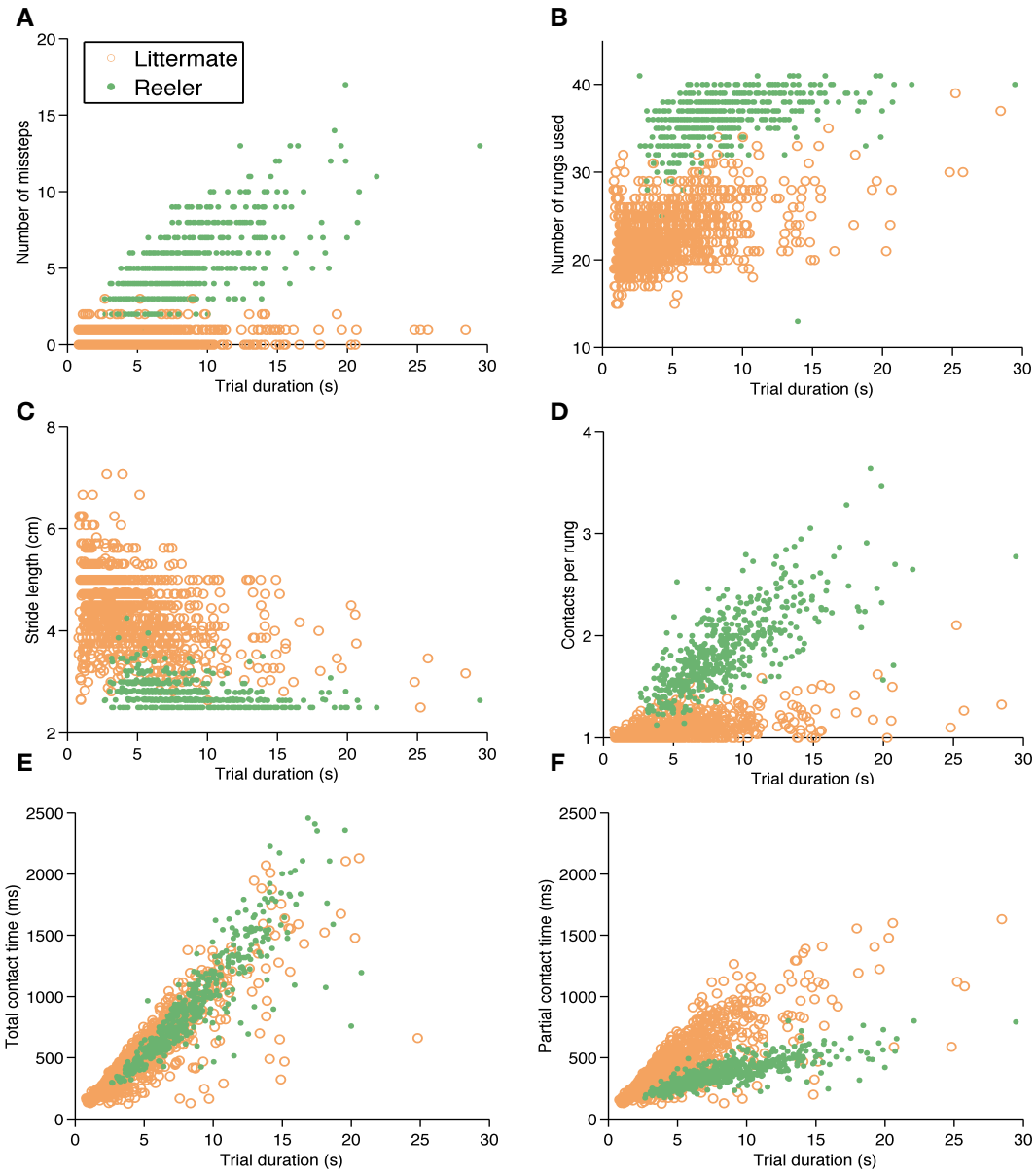

Figure 3.6.1: Trial duration versus locomotor parameters (raw data). Each dot represents a single trial. **A)** Number of missteps. **B)** Number of rungs used. **C)** The mean stride length of front right paw. **D)** Mean contacts per rung. **E)** Mean total contact time. **F)** Mean partial contact time. Littermates – orange open circles; Reelers – green solid dots.

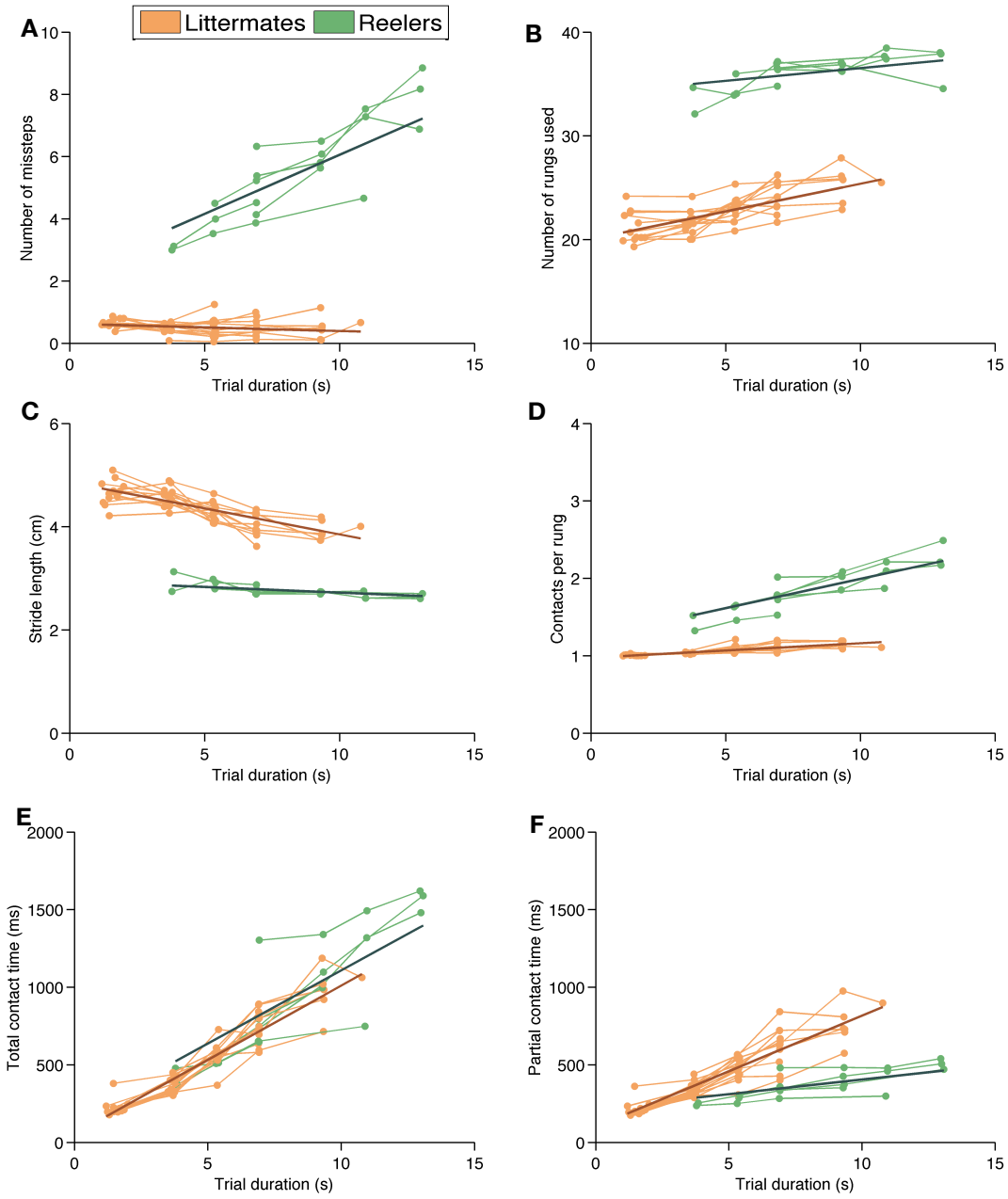

Figure 3.6.2: Trial duration versus locomotor parameters (per animal). Each line represents an individual animal. The fitted lines obtained from the linear mixed effects model are shown on the plots. **A)** Number of missteps. **B)** Number of rungs used. **C)** The mean stride length of front right paw. **D)** Mean contacts per rung. **E)** Mean total contact time. **F)** Mean partial contact time. Littermates – orange; Reelers – green.

3.3.3 Walking patterns and whole-body oscillations

The identification of persistent mouse walking patterns and whole-body kinematics are fundamental features necessary for understanding how mice keep their limbs coordinated and maintain balance. Therefore, we investigated specific walking patterns and whole-body oscillations displayed while mice stepped on the *LocoLadder*.

Walking patterns

The mean force sensor correlation matrix across all trials for each mouse group is shown in (Figure 3.7 A). A strikingly different correlation pattern was observed between the two groups. While littermates exhibited specific higher correlations specifically perpendicular to the matrix diagonal, reelers showed broader high correlations around the matrix diagonal. Note that matrix elements perpendicular to the matrix diagonal correspond to spatial diagonal arrangements of rungs on the ladder. These correlations between force sensors were quantified and categorized based on the rung spatial configuration (diagonal, diagonal intervaled, side-to-side, ipsilateral and ipsilateral intervaled). The mean counts for each spatial configuration across all trials are shown in (Figure 3.7 B). Although reeler mice performed significant less spatial diagonal rung configuration than control littermates, they showed other spatial rung configurations, which exhibited their deficient motor coordination.

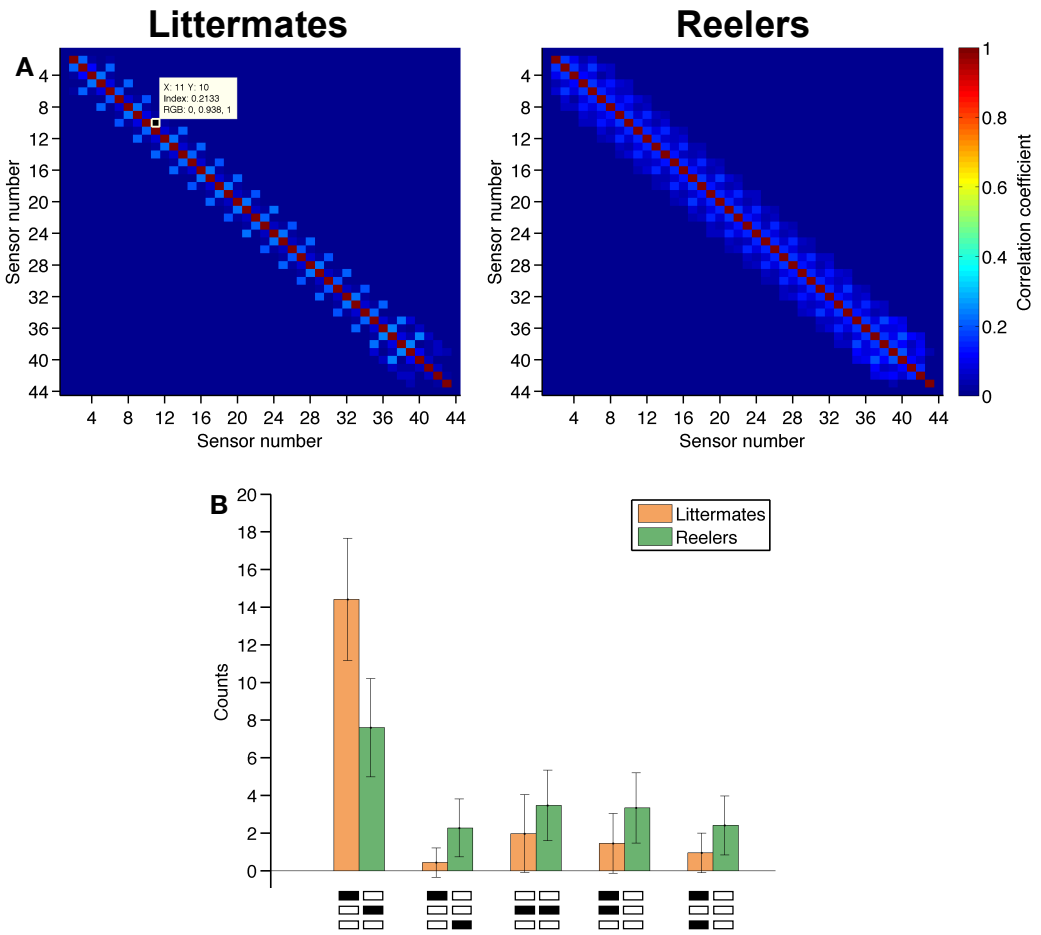

Figure 3.7: Mouse walking patterns on the ladder. **A)** Mean force sensor correlation matrix (see 3.2.2 for matrix computation). Note that the high correlation element highlighted corresponds to the rung 10 and 11 which are diagonally arranged. **B)** Mean counts for each mouse group across diagonal, diagonal intervaled, side-to-side, ipsilateral and ipsilateral intervaled spatial configurations, respectively.

Whole-body oscillations

An example trial of body center y amplitude of a representative littermate and reeler is showed in Figure 3.8 A. Reelers typically exhibited higher amplitude and prolonged body oscillations when compared to control mice. Furthermore, the quantification of the coefficient of variation showed higher amplitude variability in reeler mice (Figure 3.8 B) **(see an example trial of side-to-side body center trajectory for both reeler and littermate – Movie 3.2).** These results exhibited reelers inability to maintain their body centered to the ladder while performing the task.

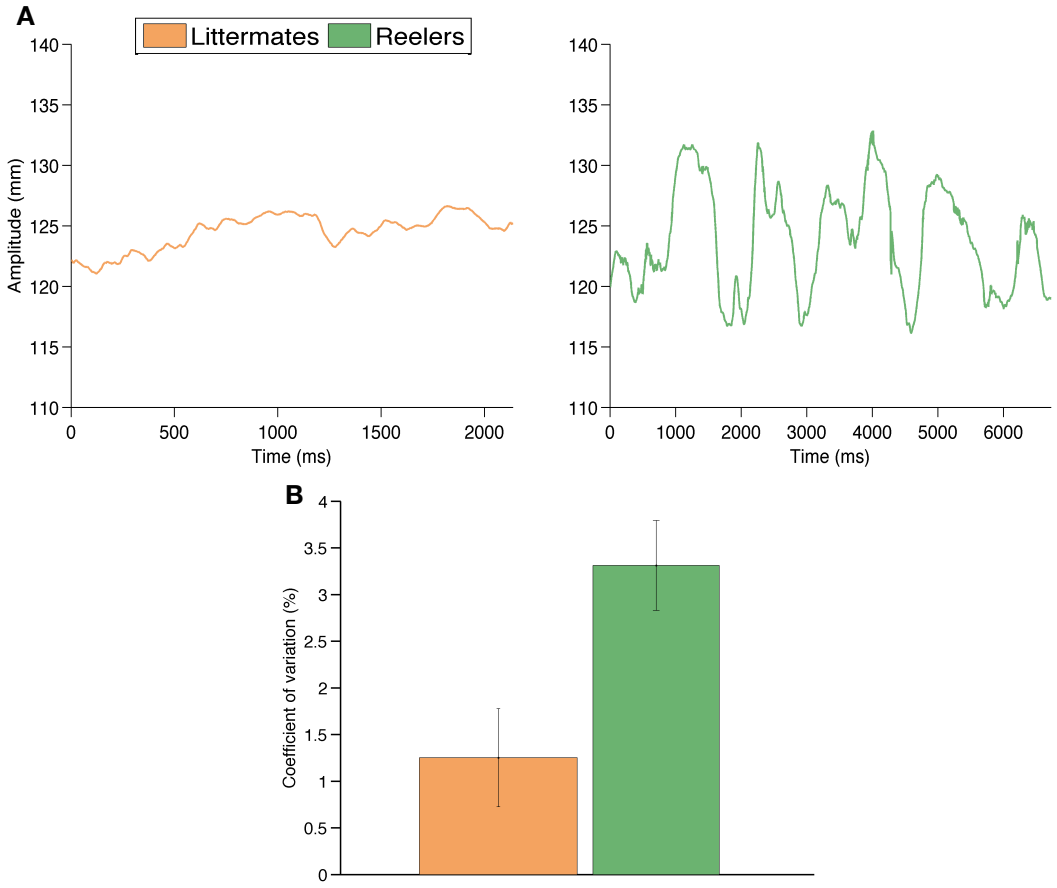

Figure 3.8: Body center y oscillations. **A)** Example trial of y body center trajectory of a representative littermate (orange) and reeler (green) mouse. **B)** Quantification of the coefficient of variation of both groups (see Appendix III for more detailed information on body center detection and Section 3.2.2 for the coefficient of variation computation).

3.3.4 Ground reaction forces signatures

Finally, we aimed to study the load profiles during paw-rung contact, their dependence on walking speed and to identify possible individual signatures of each mouse group. We used body mass center displacement during the paw-rung contact as a measure of walking speed (see Section 3.2.2 for more details).

Speed dependency and tremor

The load profiles of each paw-rung contacts were analyzed for both littermate and reeler mice across different walking speeds (see Section 3.2.2 for more details on parameter computation). While in reelers the load profile looked flat across all walking speeds, in littermates, during higher walking speeds, two distinct curves emerged during paw-rung contact (Figure 3.9 A). The quantification of littermate's stance and swing onsets across speeds showed that the front and hind paw events happened within the paw-rung contact period, suggesting that these two distinct elevations corresponded to the front and hind paws weight support on the rung, respectively (Figure 3.9 B and Figure 3.10). Moreover, at higher speeds, the front swing to hind stance onset appeared farther apart in time from each other, suggesting less overlap between the front and hind paw on the rung (Figure 3.9 B).

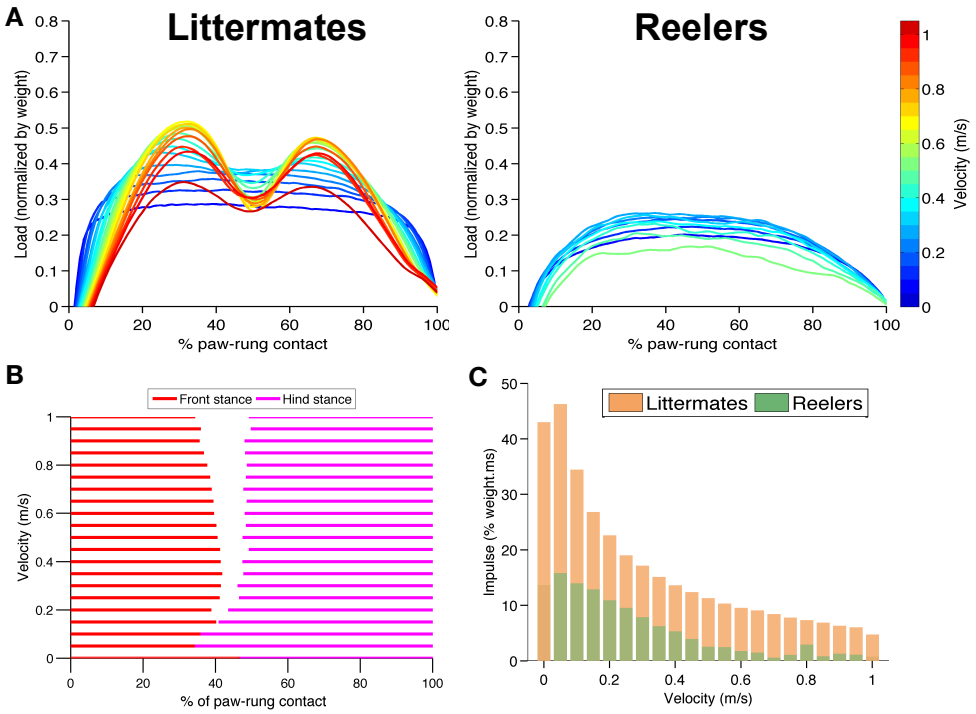

Figure 3.9: Load signatures examination. **A)** Normalized weight load profile during paw-rung contact period across different walking speeds for both groups. **B)** Littermate's front and hind stance phases across several speeds. Median swing and stance onsets were computed based on tracking information. Red – front paw stance; magenta – hind paw stance. **C)** Impulse analysis. Reelers showed lower average impulse across speed bins (0.05 m/s bin width). Impulse values were normalized by mouse's weight. See details on Section 3.2.2.

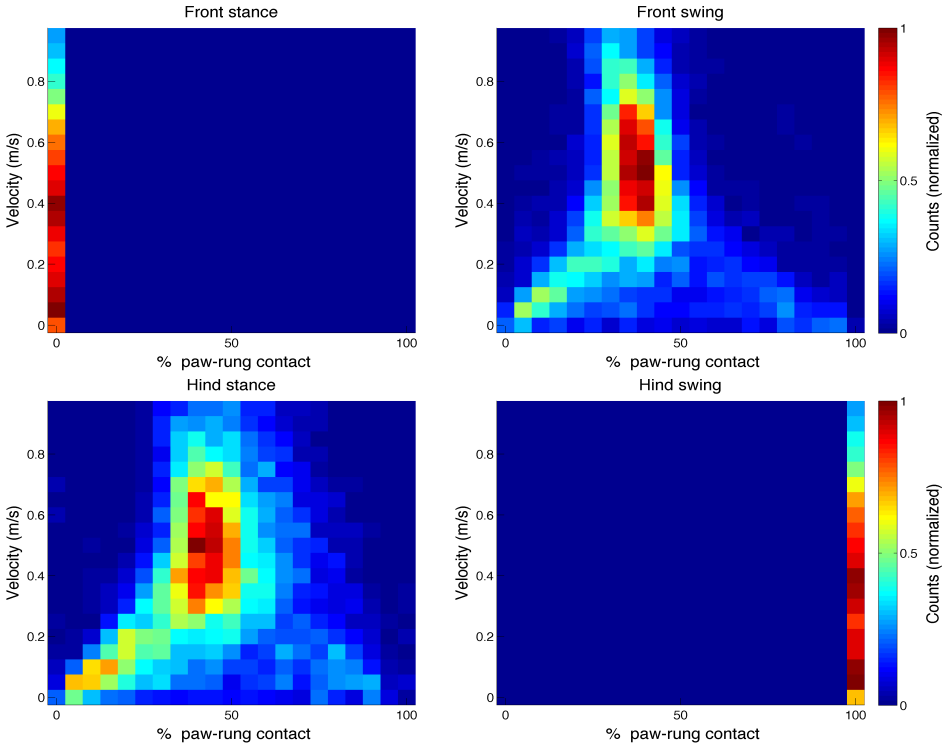

Figure 3.10: Littermate's stride cycle events onsets quantification for the front and hind paw. The front and hind paw events occurred within the paw-rung contact period. A normalized colormap histogram quantified the stance and swing onsets across several % paw-rung contact (5 % bin width) and velocity (0.05 m/s bin width) bins. See Section 3.2.2 for more details.

In addition, the load profiles for both reeler and littermate groups seemed to have different amplitudes values, (Figure 3.9 A) which was confirmed by the load impulse quantification that showed that reelers exhibited lower load impacts across different speeds (Figure 3.9 C).

Finally, we observed striking differences in the frequency analysis of the load signals. Reeler showed a marked peak at ~23 Hz at lower velocities, which was not present in control littermates (Figure 3.11). Moreover, at higher walking speeds, littermates frequency distribution exhibited an interesting peak shift from about 7 – 15 Hz not visible in the reeler mice. This frequency shift reflected the appearance of the double curve on the figure above (Figure 3.9 A).

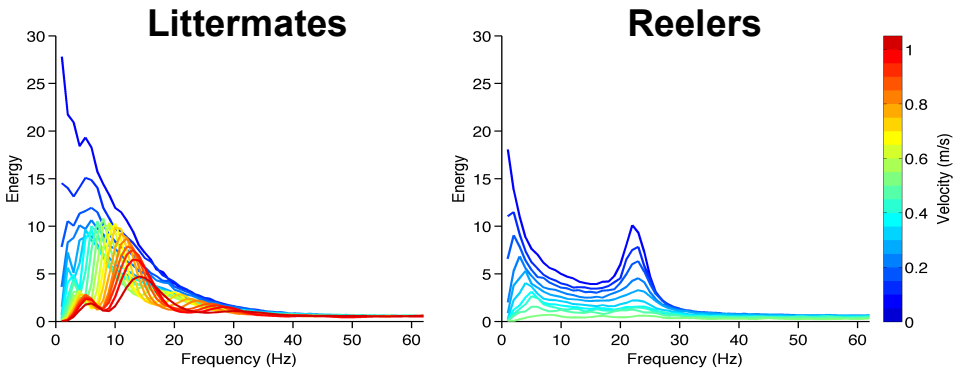

Figure 3.11: Frequency spectrum distributions across walking speeds. See load profiles details in Section 3.2.2 and frequency spectrum computation in Appendix IV.

The frequency signature of each animal was sufficient to reliably classify (>74% accuracy) (Table 3.2) the mouse type between reeler and littermate for different walking speeds (Figure 3.12).

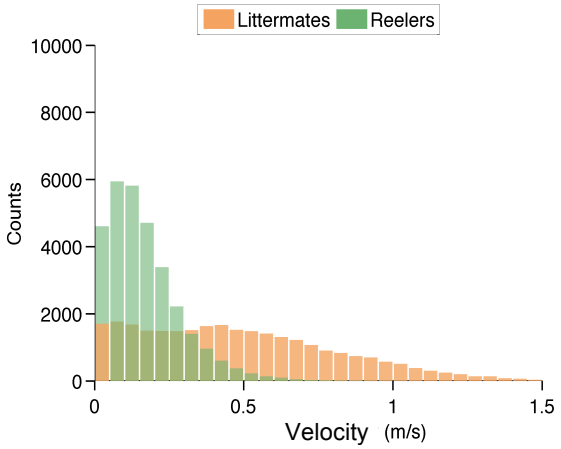

Figure 3.12: Velocity histogram. Velocity was computed using body mass center computation. Pawrung contact counts are shown for several velocity bins (0.05 m/s bin width). For the classification analysis, balanced numbers of instances of each class were selected.

Velocity (m/s)	Classification
Full data	72.64/82.32 (0.77)
0 - 0.1	72.76/75.60 (0.74)
0.1 - 0.2	74.58/75.93 (0.75)
0.2 - 0.3	73.26/77.58 (0.75)
0.3 - 0.4	74.87/80.23 (0.78)
0.4 - 0.5	81.90/83.62 (0.83)
0.5 - 0.6	86.83/87.37 (0.87)

Table 3.2: Classification parameters obtained for each velocity group. Classification: % littermates in cluster 1 / % reelers in cluster 2 and (F-measure).

3.4 Discussion

In this study, we were interested in understanding how reelers and control littermates stepped differently on a precise locomotor task. To do this, we quantified several parameters that revealed relevant global locomotion aspects. We identified a higher number of missteps, number of rungs used and increased latency to finish the task in reelers when compared with control littermates, (Figure 3.3) which reflected the low efficacy and stepping accuracy of their walking.

In order to investigate further features of mouse stepping, we measured the mouse interaction with each rung on the ladder. We found that, while control littermates showed single reaching limb movement to place their paw on each rung, reelers often exhibited additional paw-rung contacts (Figure 3.4). These multiple short duration contacts suggest failed reaching attempts to correctly place the paw on the appropriate rung. This phenotype seems consistent with two cerebellar symptoms observed in humans – *dysmetria* and *hypermetria* - which are characterized by over and under reaching targets and sudden interruptions of movements followed by exaggerated corrections.

We also aimed to understand if locomotor parameters were influenced by the mouse walking speed. We discovered that walking speed dramatically influenced the locomotor parameters assessed, (Figure 3.6.1 and Figure 3.6.2) emphasizing the need to take it to account when analyzing locomotion [49,50,54–56]. Although trial duration is an indirect measure of mouse walking speed, the slower velocities observed within reeler mice were a result of their clear severe motor deficits and not due to exploratory behavior. This reason makes trial duration a reasonable approximation to assess reeler walking speed. Although

control littermates often showed exploratory behavior, (as observed by increased variability in Figure 3.6.1 B,C and F) they indeed exhibited clear modulation with trial duration.

Furthermore, the distinct modulation of walking speed on the locomotor parameters in both groups emphasizes the clear distinction between ataxic and non-ataxic mice, with the exception of the total contact time parameter (Figure 3.6.1 E). Reeler mice showed higher variability in total contact time (Figure 3.4 C). However, for the same trial durations, the total contact time was not significantly different between the two groups, (Figure 3.6.2 E) and was also not revealed by the PCA analysis, (Table 3.1) stressing the importance of accounting for walking speed to properly analyze locomotion [49,50,54–56].

A diagonal paw patterning and appropriate whole-body positioning are two fundamental characteristics of successful motor coordination and balance. Therefore, we identified specific walking patterns and whole-body oscillations displayed while mice stepped on the ladder. We found that, reeler mice exhibited diminished diagonal patterning at the expense of other spatial patterns on the ladder, (Figure 3.7 B) highlighting their deficient ongoing motor coordination. These results are in line with whole-body coordination impairments found in a previous study that examined ataxic Purkinje cell degeneration mice during an overground walking task [54]. Moreover, while littermates kept their body centered relative to the ladder, reelers failed to maintain their posture while walking, showing marked side-to-side body movements (Figure 3.8).

In order to characterize mice walking mechanisms adopted to properly step on the ladder across several speeds, we analyzed their load signatures.
We discovered that, in contrast to littermate mice, reelers showed lower amplitudes and lacked the striking effect of walking speed on the load profile (Figure 3.9 A and C). To further elucidate this speed modulation, we combined

the tracking data with load information. We found that at higher speeds there is less overlap between the front and hind paw on the rung (Figure 3.9 B). This highly coordinated mechanism, characterized by increased 'on-air' time, enabled a smoother swing-to-stance transition of the ipsilateral front-hind paw and provided a more efficient gait needed at elevated walking velocities.

By analyzing the frequency of the load profiles, we also discovered a pronounced frequency peak around 23 Hz in reeler mice, (Figure 3.11) which suggest the presence of tremor. This typical cerebellar human sign is often associated to the so-called *intention tremors* that typically occur when a cerebellar patient attempts to stop the ongoing movement. Moreover, this result is in line with a previous study that detected tremor component in reeler mice within the frequency band of 20-25 Hz (see [44]).

Finally, we were interested in understanding if mice improved their stepping accuracy across sessions. There was no clear improvement. The parameters measured throughout the experiment, such as stride length and number of rungs used, suggested no significant learning component (Figure 3.3 B and D). Moreover, misstep quantification, which is a reliable parameter to assess the stepping accuracy, suggested no clear improvement in the accuracy of stepping across sessions (Figure 3.3 C). We hypothesize that automated misstep detection used was not sensitive enough to clearly capture learning effects that might have happened throughout the experiment. Moreover, when mice misplaced a front paw, normally the contralateral hind paw descended to the floor level to regain balance, counting as another misstep. These false-positive detections might have contributed to mask the learning component.

In summary, the low efficacy and stepping accuracy of reeler mice reflected their clear motor dysfunction. Their misplacing and the multiple short duration contacts were consistent with human cerebellar symptoms *dysmetria* and

hypermetria. Additionally, *tremor* was identified through a characteristic load frequency peak around 23 Hz. The diminished diagonal patterning and side-to-side body movements markedly exhibited their coordination and balancing problems. Finally, the walking speed dramatically influenced the locomotor parameters assessed, emphasizing the need to take it into account when analyzing locomotion.

The results shown here are in line with previous studies that reported clear motor deficits of reeler mice, including uncoordinated gait, impulsivity, tremors and balancing problems [15,21,86,87]. Due to its severe motor impairments, the complex interconnections between the cerebellum and other areas of the central nervous system and since degeneration is not restricted to just the cerebellum, we cannot make associations between specific circuit elements and the motor behavior observed. Nonetheless, the reeler locomotor profile described here, not only showed similarities with the gait observed in another cerebellar ataxic mice during overground walking [54], but also with cerebellar patients that lack a control mechanism for detecting and correcting movement errors. Specifically, we identified several motor signs in mice that are similar in cerebellar patients. In humans, these symptoms occur due to the absence of a 'motor correction system', normally leading to abnormally timed muscle activations and inability to produce smooth and well-coordinated movements [3].

Chapter 4

Conclusion and future work

4.1 Conclusions

Motor behavior is the visible result of the intricate processing that occurs in our brain. How circuit mechanisms explain motor function has been a major target of neuroscience investigation. Because the loss of motor coordination, performance, or learning is associated with many neurological conditions, there is a need to develop highly precise methods to quantify the different aspects of motor behavior. Particularly, the cerebellum is crucial for producing natural, well-coordinated movements. However, how the neural circuit computations contribute to more complex movements remain a mystery.

In this project, we developed the *LocoLadder*, a horizontal ladder paradigm for mice. The idea behind the construction of this new system was to select the most valuable tools available to quantify movement and combine them

into an important motor paradigm to study locomotor coordination. We achieved the proposed milestones:

- Access the vertical load exerted by the mouse's paws using force sensors coupled to rungs of the ladder.
- Record and track the mouse's body parts with high spatiotemporal resolution while mice freely stepped on the ladder.
- The system is easily operated by the experimenter and automated via software driven control.
- Analyzed a mutant mice with cerebellar ataxia.

Many currently used motor tasks lack specificity and sensitivity to detect subtle aspects of locomotion and are only capable of providing rather subjective measures of a particular motor function. These are often influenced by external factors, such as time to fall from a rotarod or the number of paw slips in a balance beam [31,32]. With the combination of ground reaction forces methods and gait analysis tools we were able to extract sensitive locomotion parameters while the mice freely stepped on the ladder.

Furthermore, the fully automated characterization of motor performance that we achieved with this system represents a substantial advantage compared to other ladder tasks that often rely on either semi-automatic or manual inspection that requires extensive and time-consuming analysis [58,59,66].

While the examination of gait during normal waking provides a more detailed analysis of motor coordination, the force sensors constitute a powerful tool to get insight into how these weight signatures contribute to the whole-body dynamics and locomotion. These crucial features contrast with other

sophisticated ladder paradigms such as the Erasmus ladder, that is still limited to rung binary touch detection and lacks crucial video information [88].

Importantly, using the *LocoLadder*, we successfully described the locomotor profile of reeler mice by quantifying several locomotor deficiencies:

- The low efficacy and accuracy of their stepping reflected their clear motor dysfunction.
- The misplacing and multiple short duration touches on the rungs are consistent with the human cerebellar symptoms *dysmetria* and *hypermetria.*
- *Tremor* was identified through the characteristic load frequency peak around 23 Hz.
- Diminished diagonal patterning and side-to-side body movements markedly exhibited their coordination and balancing problems.

In summary, the combination of load and gait assessment represents a significant step forward to sensitively quantify locomotor coordination in a ladder configuration. Moreover, this paradigm not only is suitable for quantification of motor coordination in mice, that is likely to be dependent upon proper function of the cerebellum, but also for other supraspinal structures that might be involved in controlling both rapid locomotor adjustments and motor learning while an animal walks on a ladder configuration [70,73,81,83].

4.2 Future directions

The present system still has room for improvement. In the setup described, force sensors and movie acquisition were not synchronized in time, which introduced some limitations. While mice step on the ladder, they typically put their hind paw on the same rung as they have put their front paw before they move their front paw to the next rung. To fully capture this normally fast transition requires a synchronized and higher temporal resolution system that combines both load and video information. This is why we are developing an acquisition board that will synchronize both acquisition and increase force sensor temporal resolution to reliably divide the load profile during paw-rung contact time into stance and swing time. Indeed, this improved system will provide the assessment to individual hind and front paw characteristics and enhance our chances of detecting even more subtle locomotor phenotypes.

Although misstep detection worked reliably to evaluate overall mouse motor performance, because it was for now limited to sensor information, it lacked specificity regarding how these missteps happened. A mouse might have touched the floor when they misstepped, when their paws descend to the floor level to maintain balance or when it stops to explore the apparatus. Synchronous and improved tracking information is needed to increase the sensitivity of the misstep detection, and to provide further information on any learning component that might happen throughout an experiment. Furthermore, we will change the floor of the ladder from the light acrylic material used to a solid glass floor. This way, it will remove variability in the signal measured (due to the material vibration) and consequently, enhance misstep detection.

More recently, there has been an exponential development of new methods to manipulate neural circuits. These modern neuroengineering techniques merge

genetic and optical systems (optogenetics) to reversibly stimulate and inhibit particular neurons within a specific neural circuit [89].

The integrated acquisition board that we are currently developing will not only synchronize both camera and sensor acquisition but will enable force-sensor optogenetic triggering. With this technology, we will be able to select specific rungs that will control the optogenetic laser, enabling accurate information about motor timing in relation to changes in neural activity. Such a system combined with new optogenetic tools should yield relevant details about motor control and provide new means of understanding how the cerebellum contributes to skilled locomotion.

Appendices

Appendix I

Sensor activation detection algorithm

This algorithm aimed at extracting touch duration of individual rung activation (first and last timestamp of each activation) from the load data generated in each trial. Moreover, using tracking information we developed an additional processing step to avoid sensor activation triggered by body parts other than the paws. The algorithm was divided into two main phases:

I.I Touch event detection

After importing the data, the next processing steps were performed on each individual force sensor signal:

- Subtraction of the previously registered baseline value of the load signal (see Section 2.5 for details on baseline acquisition).
- Detection of load values > 0.001 mV/V (Figure A.1 A).
- Intensity to weight conversion using calibration function (see Section 2.2.1 for more details on calibration function computation).
- Detection of touches based on the following criteria: minimum load >1 gram and minimum touch duration > 20 ms.

- A touch was considered independent of another touch if it had a separation > 50 ms.
- Touch events indexes were saved.

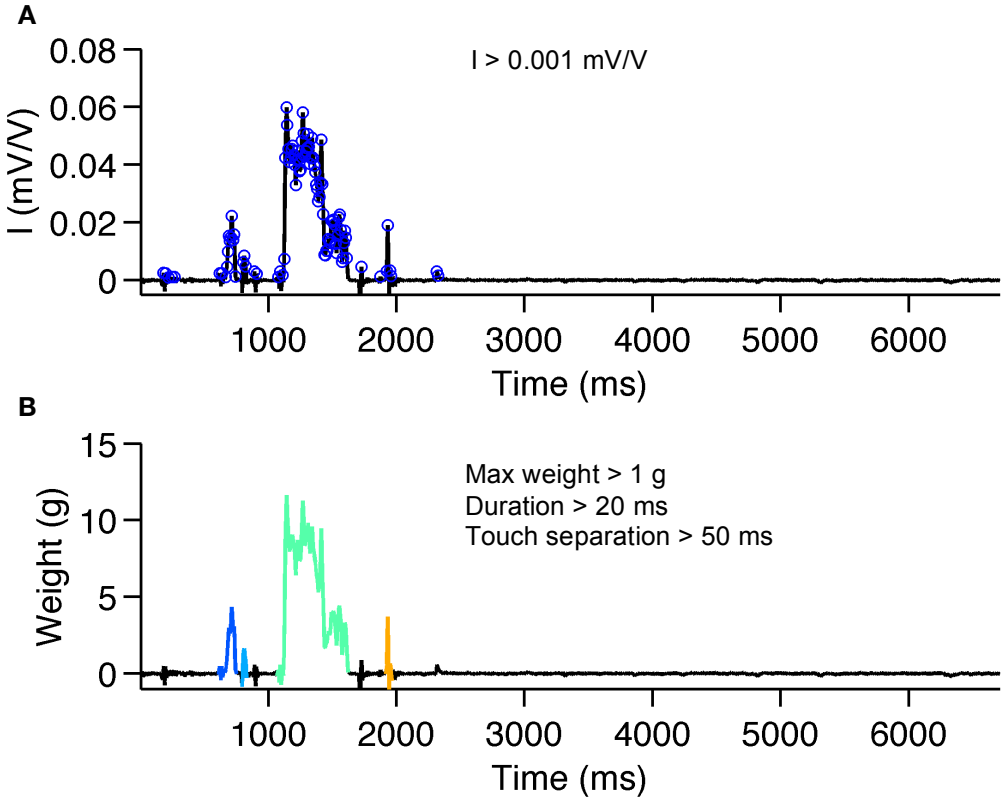

Figure A.1: Touch event detection of an example trial of a reeler. **A)** Load values detection with intensity > 0.001 mV/V. **B)** Touch selection based on criteria. Intensity to weight conversion. Each colored line represents an independent touch.

I.II Filtering using tracking information

The abnormal walking of reeler mice reduced the ability to reliably track the mouse's paws. However, we thought that it would still be useful to eliminate rung touches triggered by other body parts, both in reelers and control mice. Using forward paw trajectories, we limited the time in which a sensor could be active. This constraint was defined by a spatial window in which paws had to be present. Thus, when the paws are present within this spatial window, it would likely

represent a paw touch on that sensor. To do this, we defined specific regions for each rung (illustrated by the white rectangles in Figure A.2 A). Thus, for each sensor, we got a time constraint defined by the spatial windows of activation (represented by each black trace superimposed on the colored lines in Figure A.2 B). Finally, for each sensor, we filtered out load signals outside the spatial window (Figure A.2 C).

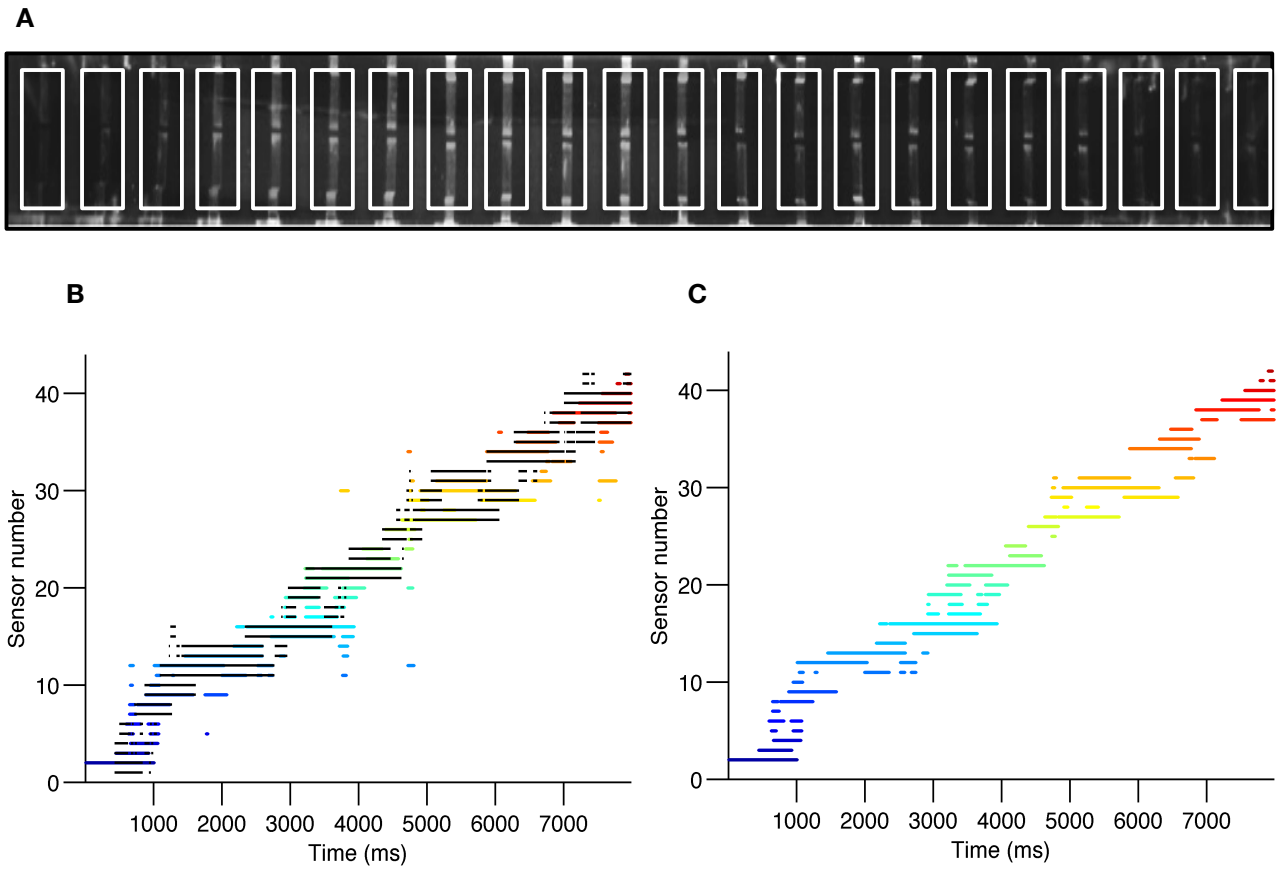

Figure A.2: Activation filtering based on tracking information. **A)** Illustration of the spatial regions defined for each rung (approx. 8 mm before and after the rung). **B)** Unfiltered load events of an example reeler mouse trial. Each line color represents the load activation period of each 44 sensors. The black traces represent the time constraints obtained from the spatial windows. **C)** Filtered load touches.

Appendix II

Misstep detection

To detect missteps on the ladder, we used the two sensors built in the transparent acrylic floor 1.5 cm below the rungs of the ladder. The sensors are located 15 cm from either end of the corridor. Because a mouse misstep caused different amplitudes on both sensors (due to the different relative distances to the sensors) we computed the average of these two signals and used it for misstep detection. When mice stepped on the floor below the ladder, a negative change occurred due the inverted orientation of the load cells below the rungs (contrasting to the positive change of the sensors coupled to the rungs) (Figure A.3). The signal was then smoothed with a gaussian filter with a temporal window of 80 ms. Missteps were detected by identifying the negative peaks of this signal using a minimum peak height of 0.0005 s^{-1} and mean peak distance of 500 ms.

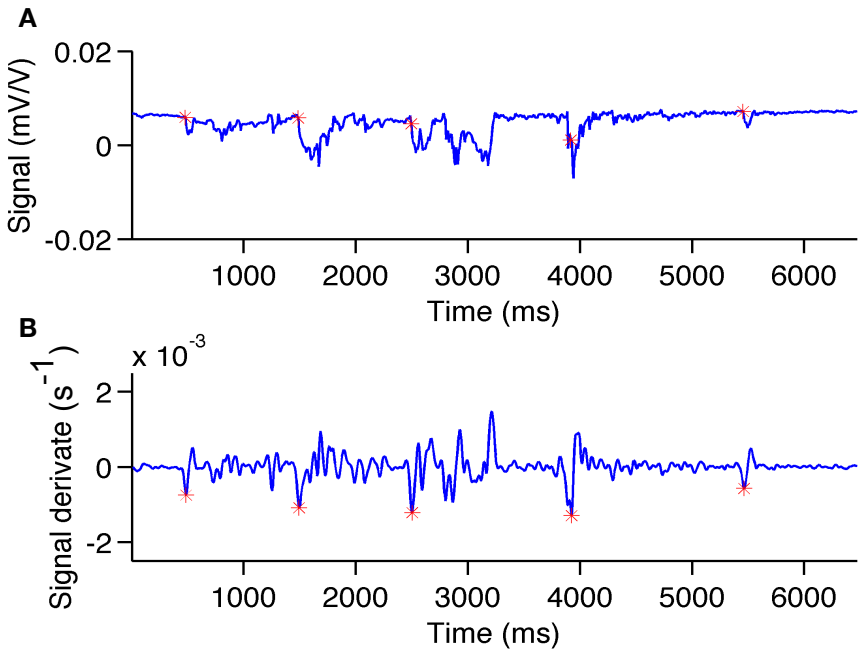

Figure A.3: Misstep detection of an example trial of a reeler. **A)** Average signal of the two sensors embedded on the ladder. **B)** Derivative of the signal after application of a gaussian filter with 80 ms width window.

Appendix III

Body mass center computation

The body mass center (x and y coordinates) were obtained taking advantage of the recorded movie while mice walked through the corridor **(see an example of body center trajectory for both reeler and littermate – Movie 3.2).** In a frame-by-frame manner, we performed the following computations on the bottom-view image (Figure A.4):

- Subtracted the background image obtained in the beginning of each trial.
- Exponentiation operation by computing the square of pixel intensity values (I^2) with subsequent normalization between 0-255.
- Conversion to binary image using a 0.2 threshold.
- Object filling operation on the binary image.
- Removal of unconnected objects with an area <10 pixels.
- Identification of the largest connected component (using 8-connected objects).
- Computation of the x and y coordinates of the centroid.

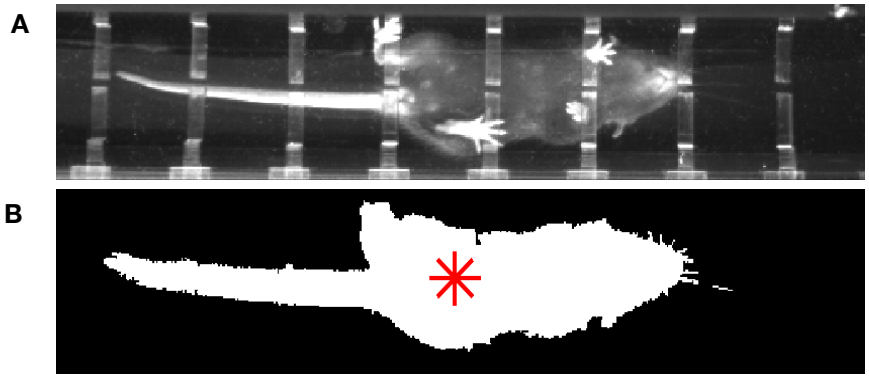

Figure A.4: Body mass center computation. **A)** Original image. **B)** The result after morphological and image processing operations. Computed centroid represented in red.

Appendix IV

Frequency energy spectrum analysis

To investigate the presence of tremor we performed a wavelet analysis on the load profiles of each paw-rung contact. A Morlet wavelet method was used with a sampling frequency of 62.5 Hz (Nyquist frequency of the force signal). Furthermore, we choose a high cycle number (100) in the wavelet in order to get a high-frequency resolution (what we were interested in quantifying) at the expense of a low temporal resolution. For each paw-rung contact, (example in red) a time-frequency spectrum was generated (Figure A.5). Following this, a time summation (sum of each line) was performed and an energy spectral density distribution was obtained. With this analysis, we obtained the relative contribution of each frequency component to the load profile signal.

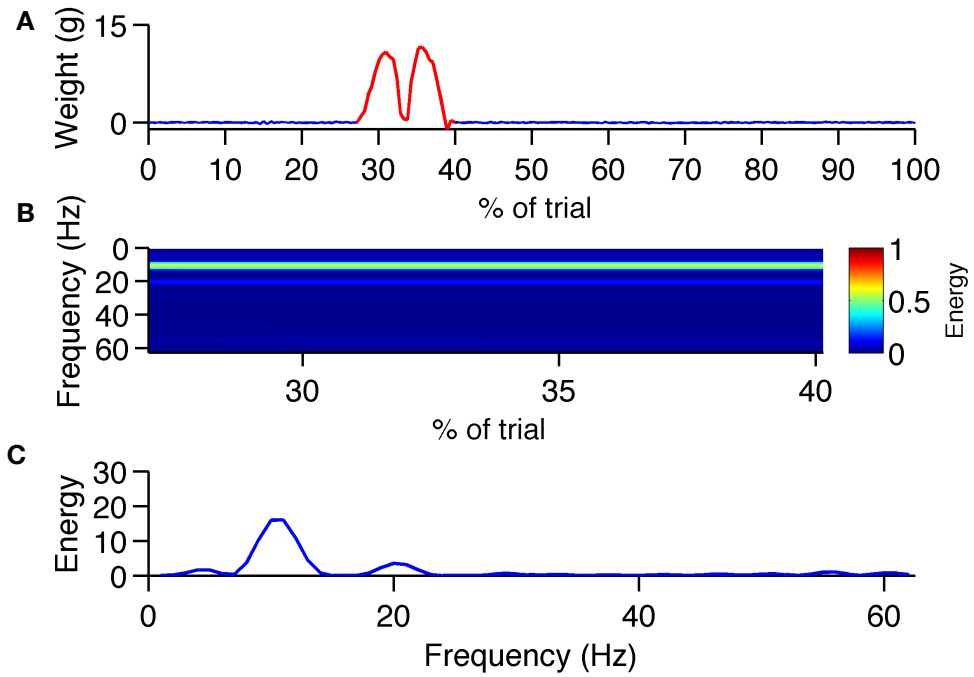

Figure A.5: Frequency distribution of a littermate load profile. **A)** Force sensor signal with the load profile highlighted in red. **B)** Time-frequency spectrum of the load profile. Time is shown in percentage of the trial. Energy units normalized to 0-1 values. **C)** Frequency distribution obtained from time summation of the time-frequency matrix.

References

[1] "IBM100 - Deep Blue," 07-Mar-2012. [Online]. Available: http://www-03.ibm.com/ibm/history/ibm100/us/en/icons/deepblue/. [Accessed: 10-Dec-2015].

[2] H. Ritter and R. Haschke, "Hands, Dexterity, and the Brain." CRC Press/Taylor & Francis, 2015.

[3] E. Kandel, J. Schwartz, T. Jessel, S. Siegelbaum, and A. Hudspeth, *Principles of Neural Science*, 5th ed. McGraw-Hill Companies, 2013.

[4] D. S. Reisman, H. J. Block, and A. J. Bastian, "Interlimb coordination during locomotion: what can be adapted and stored?," *J. Neurophysiol.*, vol. 94, no. 4, pp. 2403–2415, 2005.

[5] D. Purves, G. J. Augustine, D. Fitzpatrick, L. C. Katz, A.-S. LaMantia, J. O. McNamara, and S. M. Williams, "Neuroscience." Sinauer Associates, 2001.

[6] W. E. Crusio, *Mouse behavioral testing. How to use mice in behavioral research - by Douglas Wahlsten*, vol. 12, no. 2. 2013.

[7] D. a E. Bolton, a. D. Y. Tse, M. Ballermann, J. E. Misiaszek, and K. Fouad, "Task specific adaptations in rat locomotion: Runway versus horizontal ladder," *Behav. Brain Res.*, vol. 168, no. 2, pp. 272–279, 2006.

[8] G. a. Metz and I. Q. Whishaw, "Cortical and subcortical lesions impair skilled walking in the ladder rung walking test: A new task to evaluate fore- and hindlimb stepping, placing, and co-ordination," *J. Neurosci. Methods*, vol. 115, no. 2, pp. 169–179, 2002.

[9] M. Mauk and W. Thach, "The Cerebellum," 3 edition., Elvesier, Ed. Inc, 2008, pp. 751–774.

[10] J. L. Raymond, S. G. Lisberger, and M. D. Mauk, "The cerebellum: a neuronal learning machine?," *Science*, vol. 272, no. 5265, pp. 1126–1131, 1996.

[11] S. M. Morton and A. J. Bastian, "Mechanisms of cerebellar gait ataxia.," *Cerebellum*, vol. 6, no. 1, pp. 79–86, 2007.

[12] M. Coesmans, P. a S. Smitt, D. J. Linden, R. Shigemoto, T. Hirano, Y. Yamakawa, A. M. van Alphen, C. Luo, J. N. van der Geest, J. M. Kros, C. a Gaillard, M. a Frens, and C. I. de Zeeuw, "Mechanisms underlying cerebellar motor deficits due to mGluR1-autoantibodies.," *Ann. Neurol.*, vol. 53, no. 3, pp. 325–36, 2003.

[13] W. Ilg, M. a Giese, E. R. Gizewski, B. Schoch, and D. Timmann, "The influence of focal cerebellar lesions on the control and adaptation of gait.," *Brain*, vol. 131, no. Pt 11, pp. 2913–27, 2008.

[14] T. van der Vaart, G. M. van Woerden, Y. Elgersma, C. I. de Zeeuw, and M. Schonewille, "Motor deficits in neurofibromatosis type 1 mice: The role of the cerebellum," *Genes,*

Brain Behav., vol. 10, no. 4, pp. 404–409, 2011.

[15] J. Cendelin, "From mice to men: lessons from mutant ataxic mice," *Cerebellum & Ataxias*, vol. 1, no. 1, p. 4, 2014.

[16] D. T. H. Lai, R. K. Begg, and M. Palaniswami, "Computational intelligence in gait research: a perspective on current applications and future challenges.," *IEEE Trans. Inf. Technol. Biomed.*, vol. 13, no. 5, pp. 687–702, 2009.

[17] V. Cimolin and M. Galli, "Summary measures for clinical gait analysis: A literature review," *Gait Posture*, vol. 39, no. 4, pp. 1005–1010, 2014.

[18] T. D. B. Nguyen-Vu, R. R. Kimpo, J. M. Rinaldi, A. Kohli, H. Zeng, K. Deisseroth, and J. L. Raymond, "Cerebellar Purkinje cell activity drives motor learning.," *Nat. Neurosci.*, vol. 16, no. 12, pp. 1734–6, 2013.

[19] C. I. De Zeeuw, C. Hansel, F. Bian, S. K. E. Koekkoek, A. M. van Alphen, D. J. Linden, and J. Oberdick, "Expression of a Protein Kinase C Inhibitor in Purkinje Cells Blocks Cerebellar LTD and Adaptation of the Vestibulo-Ocular Reflex," *Neuron*, vol. 20, no. 3, pp. 495–508, 1998.

[20] M. Schonewille, A. Belmeguenai, S. K. Koekkoek, S. H. Houtman, H. J. Boele, B. J. van Beugen, Z. Gao, A. Badura, G. Ohtsuki, W. E. Amerika, E. Hosy, F. E. Hoebeek, Y. Elgersma, C. Hansel, and C. I. De Zeeuw, "Purkinje cell-specific knockout of the protein phosphatase PP2B impairs potentiation and cerebellar motor learning.," *Neuron*, vol. 67, no. 4, pp. 618–28, Aug. 2010.

[21] R. Lalonde and C. Strazielle, "Spontaneous and induced mouse mutations with cerebellar dysfunctions: Behavior and neurochemistry," *Brain Res.*, vol. 1140, no. 1, pp. 51–74, 2007.

[22] R. J. Mullen, E. M. Eicher, and R. L. Sidman, "Purkinje cell degeneration, a new neurological mutation in the mouse.," *Proc. Natl. Acad. Sci. U. S. A.*, vol. 73, no. 1, pp. 208–12, Jan. 1976.

[23] J. T. Walter, K. Alviña, M. D. Womack, C. Chevez, and K. Khodakhah, "Decreases in the precision of Purkinje cell pacemaking cause cerebellar dysfunction and ataxia.," *Nat. Neurosci.*, vol. 9, no. 3, pp. 389–97, Mar. 2006.

[24] A. Spink, L. Noldus, and P. Zimmerman, "Measuring Behavior 2008," in *Proceedings of Measuring Behavior 2008, 6th International Conference on Methods and Techniques in Behavioral Research*, p. 55.

[25] B. J. Cummings, C. Engesser-Cesar, G. Cadena, and A. J. Anderson, "Adaptation of a ladder beam walking task to assess locomotor recovery in mice following spinal cord injury.," *Behav. Brain Res.*, vol. 177, no. 2, pp. 232–41, Feb. 2007.

[26] K. L. McIlwain, M. Y. Merriweather, L. A. Yuva-Paylor, and R. Paylor, "The use of behavioral test batteries: effects of training history," *Physiol Behav*, vol. 73, pp. 705–717, 2001.

[27] D. C. Rogers, E. M. C. Fisher, S. D. M. Brown, J. Peters, A. J. Hunter, and J. E. Martin, "Behavioral and functional analysis of mouse phenotype: SHIRPA, a proposed protocol for comprehensive phenotype assessment," *Mamm. Genome*, vol. 8, no. 10, pp. 711–713, Oct. 1997.

[28] S. P. Brooks and S. B. Dunnett, "Tests to assess motor phenotype in mice: a user's guide.," *Nat. Rev. Neurosci.*, vol. 10, no. 7, pp. 519–529, 2009.

[29] K. S. Tatem, J. L. Quinn, A. Phadke, Q. Yu, H. Gordish-Dressman, and K. Nagaraju, "Behavioral and Locomotor Measurements Using an Open Field Activity Monitoring System for Skeletal Muscle Diseases," *J. Vis. Exp.*, no. 91, p. e51785, 2014.

[30] C. M. Novak, P. R. Burghardt, and J. A. Levine, "The use of a running wheel to measure activity in rodents: Relationship to energy balance, general activity, and reward," *Neurosci. Biobehav. Rev.*, vol. 36, no. 3, pp. 1001–1014, 2012.

[31] T. N. Luong, H. J. Carlisle, A. Southwell, and P. H. Patterson, "Assessment of Motor Balance and Coordination in Mice using the Balance Beam," *J. Vis. Exp.*, no. 49, pp. 7–9, 2011.

[32] R. M. J. Deacon, "Measuring motor coordination in mice.," *J. Vis. Exp.*, no. 75, p. e2609, 2013.

[33] S. Stroobants, I. Gantois, T. Pooters, and R. D'Hooge, "Increased gait variability in mice with small cerebellar cortex lesions and normal rotarod performance.," *Behav. Brain Res.*, vol. 241, pp. 32–7, 2013.

[34] A. Can, D. T. Dao, M. Arad, C. E. Terrillion, S. C. Piantadosi, and T. D. Gould, "The Mouse Forced Swim Test," *J. Vis. Exp.*, no. 58, pp. 4–8, 2011.

[35] M.-W. Chang, C.-P. Chang, Y.-C. Wei, S.-Y. Hou, M.-S. Young, and M.-T. Lin, "A force plate measurement system to assess hindlimb weight support of spinal cord injured rats," *J. Neurosci. Methods*, vol. 189, no. 1, pp. 130–137, 2010.

[36] J. M. Welch, J. a. Wade, B. M. Hillberry, and C. M. Weaver, "Force platform for rats measures fore and hind forces concurrently," *J. Biomech.*, vol. 42, no. 16, pp. 2734–2738, 2009.

[37] S. C. Fowler and N. a. Muma, "Use of a force-sensing automated open field apparatus in a longitudinal study of multiple behavioral deficits in CAG140 Huntington's disease model mice," *Behav. Brain Res.*, vol. 294, pp. 7–16, 2015.

[38] S. C. Fowler, B. R. Birkestrand, R. Chen, S. J. Moss, E. Vorontsova, G. Wang, and T. J. Zarcone, "A force-plate actometer for quantitating rodent behaviors: illustrative data on locomotion, rotation, spatial patterning, stereotypies, and tremor," *J. Neurosci. Methods*, vol. 107, no. 1–2, pp. 107–124, 2001.

[39] J. J. Chiesa, J. F. Araujo, and A. Díez-Noguera, "Method for studying behavioural activity patterns during long-term recordings using a force-plate actometer," *J. Neurosci. Methods*, vol. 158, no. 1, pp. 157–168, 2006.

[40] A. a Webb, B. Kerr, T. Neville, S. Ngan, and H. Assem, "Kinematics and ground reaction force determination: a demonstration quantifying locomotor abilities of young adult, middle-aged, and geriatric rats.," *J. Vis. Exp.*, no. 48, pp. 1–5, 2011.

[41] K. a. Clarke, "Differential fore- and hindpaw force transmission in the walking rat," *Physiol. Behav.*, vol. 58, no. 3, pp. 415–419, 1995.

[42] A. C. Zumwalt, M. Hamrick, and D. Schmitt, "Force plate for measuring the ground reaction forces in small animal locomotion," *J. Biomech.*, vol. 39, no. 15, pp. 2877–2881, 2006.

[43] M. Silvennoinen, T. Rantalainen, and H. Kainulainen, "Validation of a method to measure total spontaneous physical activity of sedentary and voluntary running mice.," *J. Neurosci. Methods*, vol. 235, pp. 51–8, 2014.

[44] D. Campolo, G. Cavallo, F. Keller, D. Accoto, P. Dario, and E. Guglielmelli, "Design and development of a miniaturized 2-axis force sensor for tremor analysis during locomotion in small-sized animal models.," *Conf. Proc. IEEE Eng. Med. Biol. Soc.*, vol. 5, pp. 5054–7, 2005.

[45] K. a Clarke and J. Still, "Gait analysis in the mouse.," *Physiol. Behav.*, vol. 66, no. 5, pp. 723–729, 1999.

[46] G. D. Muir and I. Q. Whishaw, "Ground reaction forces in locomoting hemi-parkinsonian rats: A definitive test for impairments and compensations," *Exp. Brain Res.*, vol. 126, no. 3, pp. 307–314, 1999.

[47] B. J. H. Smith, L. Cullingford, and J. R. Usherwood, "Identification of mouse gaits using a novel force-sensing exercise wheel," *J. Appl. Physiol.*, vol. 119, no. 6, pp. 704–718, 2015.

[48] G. A. Cavagna, N. C. Heglund, and C. R. Taylor, "Mechanical work in terrestrial

locomotion: two basic mechanisms for minimizing energy expenditure.," *Am. J. Physiol.*, vol. 233, no. 5, pp. R243–61, Nov. 1977.

[49] N. D. Neckel, "Methods to Quantify the Velocity Dependence of Common Gait Measurements from Automated Rodent Gait Analysis Devices," *J. Neurosci. Methods*, vol. 253, pp. 244–253, 2015.

[50] J. Cendelín, J. Voller, and F. Vozeh, "Ataxic gait analysis in a mouse model of the olivocerebellar degeneration.," *Behav. Brain Res.*, vol. 210, no. 1, pp. 8–15, Jun. 2010.

[51] F. P. T. Hamers, G. C. Koopmans, and E. a J. Joosten, "CatWalk-assisted gait analysis in the assessment of spinal cord injury.," *J. Neurotrauma*, vol. 23, no. 3–4, pp. 537–548, 2006.

[52] T. G. Hampton, M. R. Stasko, A. Kale, I. Amende, and A. C. S. Costa, "Gait dynamics in trisomic mice: quantitative neurological traits of Down syndrome.," *Physiol. Behav.*, vol. 82, no. 2–3, pp. 381–9, Sep. 2004.

[53] B. Zörner, L. Filli, M. L. Starkey, R. Gonzenbach, H. Kasper, M. Röthlisberger, M. Bolliger, and M. E. Schwab, "Profiling locomotor recovery: comprehensive quantification of impairments after CNS damage in rodents.," *Nat. Methods*, vol. 7, no. August, pp. 701–708, 2010.

[54] A. S. Machado, D. M. Darmohray, J. Fayad, H. G. Marques, and M. R. Carey, "A quantitative framework for whole-body coordination reveals specific deficits in freely walking ataxic mice.," *Elife*, vol. 4, pp. 1–22, 2015.

[55] G. C. Koopmans, R. Deumens, G. Brook, J. Gerver, W. M. M. Honig, F. P. T. Hamers, and E. A. J. Joosten, "Strain and locomotor speed affect over-ground locomotion in intact rats.," *Physiol. Behav.*, vol. 92, no. 5, pp. 993–1001, Dec. 2007.

[56] R. J. Batka, T. J. Brown, K. P. Mcmillan, R. M. Meadows, K. J. Jones, and M. M. Haulcomb, "The need for speed in rodent locomotion analyses.," *Anat. Rec. (Hoboken).*, vol. 297, no. 10, pp. 1839–64, Oct. 2014.

[57] S. M. Morton and A. J. Bastian, "Cerebellar contributions to locomotor adaptations during splitbelt treadmill walking.," *J. Neurosci.*, vol. 26, no. 36, pp. 9107–9116, 2006.

[58] J. B. Carmel, L. J. Berrol, M. Brus-Ramer, and J. H. Martin, "Chronic Electrical Stimulation of the Intact Corticospinal System after Unilateral Injury Restores Skilled Locomotor Control and Promotes Spinal Axon Outgrowth," *J. Neurosci.*, vol. 30, no. 32, pp. 10918–10926, 2010.

[59] S. G. Kanagal and G. D. Muir, "Effects of combined dorsolateral and dorsal funicular lesions on sensorimotor behaviour in rats," *Exp. Neurol.*, vol. 214, no. 2, pp. 229–239, 2008.

[60] A. a. Webb and G. D. Muir, "Unilateral dorsal column and rubrospinal tract injuries affect overground locomotion in the unrestrained rat," *Eur. J. Neurosci.*, vol. 18, no. 2, pp. 412–422, 2003.

[61] G. a Metz, D. Merkler, V. Dietz, M. E. Schwab, and K. Fouad, "Efficient testing of motor function in spinal cord injured rats.," *Brain Res.*, vol. 883, no. 2, pp. 165–177, 2000.

[62] A. Pajoohesh-Ganji, K. R. Byrnes, G. Fatemi, and A. Faden, "A combined scoring method to assess behavioral recovery after mouse spinal cord injury," *Neurosci. Res.*, vol. 67, no. 2, pp. 117–125, 2010.

[63] M. R. Hunsaker, R. E. von Leden, B. T. Ta, N. J. Goodrich-Hunsaker, G. Arque, K. Kim, R. Willemsen, and R. F. Berman, "Motor deficits on a ladder rung task in male and female adolescent and adult CGG knock-in mice," *Behav. Brain Res.*, vol. 222, no. 1, pp. 117–121, 2011.

[64] A. Encarnacion, N. Horie, H. Keren-Gill, T. M. Bliss, G. K. Steinberg, and M. Shamloo, "Long-term behavioral assessment of function in an experimental model for ischemic stroke.," *J. Neurosci. Methods*, vol. 196, no. 2, pp. 247–57, 2011.

[65] J. S. Soblosky, L. L. Colgin, D. Chorney-Lane, J. F. Davidson, and M. E. Carey, "Ladder beam and camera video recording system for evaluating forelimb and hindlimb deficits after sensorimotor cortex injury in rats," *J. Neurosci. Methods*, vol. 78, no. 1–2, pp. 75–83, 1997.

[66] H. Majczyński, K. Maleszak, T. Górska, and U. Sławińska, "Comparison of two methods for quantitative assessment of unrestrained locomotion in the rat," *J. Neurosci. Methods*, vol. 163, no. 2, pp. 197–207, 2007.

[67] I. Antonow-Schlorke, J. Ehrhardt, and M. Knieling, "Modification of the ladder rung walking task - New options for analysis of skilled movements," *Stroke Res. Treat.*, vol. 2013, 2013.

[68] L. J. G. Bouyer, "Contribution of Cutaneous Inputs From the Hindpaw to the Control of Locomotion. I. Intact Cats," *J. Neurophysiol.*, vol. 90, no. 6, pp. 3625–3639, 2003.

[69] G. a Metz and I. Q. Whishaw, "The ladder rung walking task: a scoring system and its practical application.," *J. Vis. Exp.*, no. 28, pp. 2–5, 2009.

[70] M. H. Canu and C. Garnier, "A 3D analysis of fore- and hindlimb motion during overground and ladder walking: Comparison of control and unloaded rats," *Exp. Neurol.*, vol. 218, no. 1, pp. 98–108, 2009.

[71] T. D. Farr, L. Liu, K. L. Colwell, I. Q. Whishaw, and G. a. Metz, "Bilateral alteration in stepping pattern after unilateral motor cortex injury: A new test strategy for analysis of skilled limb movements in neurological mouse models," *J. Neurosci. Methods*, vol. 153, no. 1, pp. 104–113, 2006.

[72] J. Cendelín, I. Korelusová, and F. Vožeh, "The Effect of Cerebellar Transplantation and Enforced Physical Activity on Motor Skills and Spatial Learning in Adult Lurcher Mutant Mice," *Cerebellum*, vol. 8, no. 1, pp. 35–45, 2009.

[73] a Amos, D. M. Armstrong, and D. E. Marple-Horvat, "A ladder paradigm for studying skilled and adaptive locomotion in the cat.," *J. Neurosci. Methods*, vol. 20, no. 4, pp. 323–340, 1987.

[74] G. Andersson and D. M. Armstrong, "Complex spikes in Purkinje cells in the lateral vermis (b zone) of the cat cerebellum during locomotion.," *J. Physiol.*, vol. 385, pp. 107–134, 1987.

[75] D. E. Marple-Horvat and J. M. Criado, "Rhythmic neuronal activity in the lateral cerebellum of the cat during visually guided stepping," *J. Physiol.*, vol. 518, no. 2, pp. 595–603, 1999.

[76] V. Marlinski, M. G. Sirota, and I. N. Beloozerova, "Differential Gating of Thalamocortical Signals by Reticular Nucleus of Thalamus during Locomotion," *J. Neurosci.*, vol. 32, no. 45, pp. 15823–15836, 2012.

[77] E. E. Stout and I. N. Beloozerova, "Differential responses of fast- and slow-conducting pyramidal tract neurons to changes in accuracy demands during locomotion.," *J. Physiol.*, vol. 591, no. Pt 10, pp. 2647–66, 2013.

[78] D. G. Wallace, S. S. Winter, and G. a. Metz, "Serial pattern learning during skilled walking," *J. Integr. Neurosci.*, vol. 11, no. 01, pp. 17–32, 2012.

[79] M. F. Vinueza Veloz, K. Zhou, L. W. J. Bosman, J.-W. Potters, M. Negrello, R. M. Seepers, C. Strydis, S. K. E. Koekkoek, and C. I. De Zeeuw, "Cerebellar control of gait and interlimb coordination.," *Brain Struct. Funct.*, 2014.

[80] M. Olsson, G. Nikkhah, C. Bentlage, and A. Björklund, "Forelimb akinesia in the rat Parkinson model: differential effects of dopamine agonists and nigral transplants as assessed by a new stepping test.," *J. Neurosci.*, vol. 15, no. 5 Pt 2, pp. 3863–75, May 1995.

[81] I. N. Beloozerova, M. G. Sirota, and H. A. Swadlow, "Activity of different classes of neurons of the motor cortex during locomotion.," *J. Neurosci.*, vol. 23, no. 3, pp. 1087–

97, Feb. 2003.

[82] M. E. Ioffe, L. A. Chernikova, and K. I. Ustinova, "Role of cerebellum in learning postural tasks.," *Cerebellum*, vol. 6, no. 1, pp. 87–94, Jan. 2007.

[83] I. N. Beloozerova and M. G. Sirota, "The role of the motor cortex in the control of accuracy of locomotor movements in the cat.," *J. Physiol.*, vol. 461, pp. 1–25, Feb. 1993.

[84] M. Molinari and L. Petrosini, "Hemicerebellectomy and motor behaviour in rats. III. Kinematics of recovered spontaneous locomotion after lesions at different developmental stages.," *Behav. Brain Res.*, vol. 54, no. 1, pp. 43–55, Mar. 1993.

[85] P. D. Nixon and R. E. Passingham, "Predicting sensory events. The role of the cerebellum in motor learning.," *Exp. brain Res.*, vol. 138, no. 2, pp. 251–7, May 2001.

[86] E. Romano, C. Michetti, A. Caruso, G. Laviola, and M. L. Scattoni, "Characterization of Neonatal Vocal and Motor Repertoire of Reelin Mutant Mice," vol. 8, no. 5, 2013.

[87] G. Laviola, E. Ognibene, E. Romano, W. Adriani, and F. Keller, "Neuroscience and Biobehavioral Reviews Gene – environment interaction during early development in the heterozygous reeler mouse : Clues for modelling of major neurobehavioral syndromes," vol. 33, pp. 560–572, 2009.

[88] A. Cupido, "Detecting Cerebellar Phenotypes with the Erasmus Ladder," Sep. 2009.

[89] F. Zhang, A. M. Aravanis, A. Adamantidis, L. de Lecea, and K. Deisseroth, "Circuit-breakers: optical technologies for probing neural signals and systems.," *Nat. Rev. Neurosci.*, vol. 8, no. 8, pp. 577–581, 2007.

[90] M. R. Carey, "Synaptic mechanisms of sensorimotor learning in the cerebellum.," *Curr. Opin. Neurobiol.*, vol. 21, no. 4, pp. 609–15, Aug. 2011.

[91] "UCLA Behavioral Testing Core - Open Field-Activity." [Online]. Available: http://btc.psych.ucla.edu/openfield.htm. [Accessed: 11-Dec-2015].

[92] "Motor Functions | Neurobehaviour Core - Lunenfeld." [Online]. Available: http://neurobehaviour.lunenfeld.ca/DEFAULT.ASP?page=Motor Functions. [Accessed: 11-Dec-2015].